Gas Separation Hot Paper

How to cite: *Angew. Chem. Int. Ed.* **2022,** *61,* e202203663
International Edition: doi.org/10.1002/anie.202203663
German Edition: doi.org/10.1002/ange.202203663

Titanium-Oxo Cluster Assisted Fabrication of a Defect-Rich Ti-MOF Membrane Showing Versatile Gas-Separation Performance

*Chen Wang, Yanwei Sun, Libo Li, Rajamani Krishna, Taotao Ji, Sixing Chen, Jiahui Yan, and Yi Liu**

Abstract: Although having shown great promise for efficient gas separation, relevant study of Ti-MOF membranes remains very scarce, owing to limited Ti source types and uncertain factors which dominate the separation properties. In this work, we pioneered the use of the $Ti_8(\mu_2\text{-}O)_8(OOCC_6H_5)_{16}$ cluster as the Ti source of MIL-125 membranes, which led to lower reaction temperature and higher missing-linker number within the framework and therefore, enhanced CO_2/N_2 adsorption selectivity. The MIL-125 membrane prepared by combining single-mode microwave heating with tertiary growth displayed an ideal CO_2/N_2 selectivity of 38.7, which ranked the highest among all pristine pure MOF membranes measured under comparable conditions. In addition, the ideal H_2/N_2 and H_2/CH_4 selectivity was as high as 64.9 and 40.7, thus showing great promise for versatile utility in gas separation.

Introduction

As an alternative to traditional energy-intensive gas separation approaches like cryogenic distillation, liquid absorption and adsorption, membrane-based gas separation has shown remarkable advantages in terms of low energy consumption, easy operation, eco-friendship and small footprint.[1] Among various materials, metal–organic frameworks (MOFs) have unique advantages in terms of tailorable pore aperture, adjustable functionality, and high surface areas. In particular, Ti-MOF has been considered a superb membrane material, owing to its excellent stability, appropriate pore size and unique adsorption behavior. MIL-125, which is representative of Ti-MOF materials, has a 3D framework with two kinds of cages (6.1 Å and 12.6 Å) and is accessible through the 5–7 Å microporous aperture. It consists of eight cyclic octamers of edge- and corner-sharing $[TiO_5(OH)]$ octahedra $Ti_8(\mu_2\text{-}O)_8(\mu_2\text{-}OH)_4$ nodes connected by 12 1,4-benzene dicarboxylate (BDC) linkers.[2] Not only the relatively large pore size of MIL-125 warrants the high diffusivity of smaller-sized gases, but also its textural and functional properties can be tailored for specific gas adsorption.[3] Caro et al.[4] first prepared NH_2-MIL-125(Ti) membranes showing decent H_2/CO_2 selectivity ($\approx$8) by secondary growth. More recently, we synthesized highly c-oriented ultrathin NH_2-MIL-125(Ti) membranes showing significantly enhanced H_2/CO_2 selectivity (24.8).[5] Nevertheless, in comparison with some extensively studied MOF (like ZIF-8, HKUST-1 and UiO-66) membranes, relevant studies on polycrystalline Ti-MOF membranes remain scarce,[5] which could be, at least partially, attributed to limited types of titanium sources. For instance, titanium isopropoxide (TPOT) has been commonly employed as titanium source of Ti-MOF. However, it suffers from fast hydrolysis even under transient exposure to moisture in the air, resulting in uncontrollable nucleation and growth rates during Ti-MOF membrane formation.[6] Alternatively, the use of layered TiS_2 as titanium source enabled better control of nucleation and growth rates of Ti-MOF membranes so that their mesoscopic structures (e.g., preferred orientation, membrane thickness, and grain boundary defects) could be precisely tuned. Nevertheless, it remained impractical to further tailor their microscopic structures (e.g., missing-linker defects, pore aperture, and pore size distribution) which in turn, may exert a more profound effect on the separation performance.

Previous studies indicated that missing-linker defects exerted a significant influence on the separation performance of MOF membranes. For instance, Zhong et al.[7] reported that diethanolamine-modified ZIF-8 membranes with abundant open metal sites displayed high C_3H_6/C_3H_8 selectivity. Park et al.[8] reported that defect-engineered UiO-66-incorporated mixed-matrix membranes exhibited exceptional C_3H_6 permeability and C_3H_6/C_3H_8 selectivity, owing to increased porosity and open metal sites caused by missing-linker defects in UiO-66 nanofillers. Very recently, we prepared highly defective UiO-66 membranes showing

[*] C. Wang, Dr. Y. Sun, T. Ji, S. Chen, J. Yan, Prof. Y. Liu
School of Chemical Engineering, State Key Laboratory of Fine Chemicals, Dalian University of Technology
Linggong Road 2, Ganjingzi District, Dalian 116024 (China)
E-mail: diligenliu@dlut.edu.cn

Prof. L. Li
College of Chemistry and Chemical Engineering, Shanxi Key Laboratory of Gas Energy Efficient and Clean Utilization, Taiyuan University of Technology
Taiyuan 030024 (China)

Prof. R. Krishna
Van 't Hoff Institute for Molecular Sciences, University of Amsterdam, Science Park 904
1098 XH Amsterdam (The Netherlands)

Prof. Y. Liu
Dalian Key Laboratory of Membrane Materials and Membrane Processes, Dalian University of Technology
Linggong Road 2, Ganjingzi District, Dalian 116024 (China)

superior CO_2/N_2 separation performance through combining ZrS_2 source with tertiary growth.[9] Inspired by the above achievements, herein we are dedicated to preparing high-performance Ti-MOF membranes through precisely tuning missing-linker defects in the framework.

The titanium-oxo cluster, which represents a member of tetravalent-transition-metal-oxo cluster family, consists of inorganic metal-oxide Ti–O–Ti cores capped with charge-compensating anions or –OH/–OH_2 pairs.[10] Decent coordinative interaction between cluster cores and charge-compensating anions renders titanium-oxo cluster the ideal metal source of Ti-MOF membranes since not only the activation energy for the formation of Ti-MOF can be significantly reduced via preorganization of cluster cores in the precursor solution which results in milder conditions for the growth of well-intergrown Ti-MOF membranes, but also missing-linker defects in the framework can be precisely tuned through manipulation of linker exchange rates which may have a positive effect on the separation performance. Park et al.[11] prepared DGIST-1 exhibiting excellent photocatalytic activity by employing $Ti_6O_6(OiPr)_6(t\text{-}BA)_6$ cluster as titanium source, which led to not only a higher degree of crystallinity but also increased accessible surface areas. Serre et al.[12] reported that the chemical environment and functionality of MIP-207 could be easily tuned through facile linker exchange with preformed $Ti_8(\mu_2\text{-}O)_8(acetate)_{12}\text{-}(formate)_4$ (Ti_8AF) cluster. Compared with conventional TPOT, using Ti_8AF cluster source led to the formation of MIP-207 particles with not only superior CO_2/N_2 adsorption selectivity but also reduced synthesis duration. Very recently, Zhang et al.[3a] synthesized FIR-125 containing $Ti_8(\mu_2\text{-}O)_8$ nodes by employing a titanium-oxo cluster as titanium source, which not only allowed easy tuning of the grain size but also gave rise to enhanced gas adsorption capacity. It should be noted that, although a titanium-oxo cluster had proven to be an ideal titanium source of Ti-MOF in powder form, there is still no report on the preparation of Ti-MOF membranes with a titanium-oxo cluster source. Motivated by potential benefits derived from the titanium-oxo cluster, herein we pioneered the use of a titanium-oxo cluster source for preparing a high-performance Ti-MOF membrane.

MIL-125 has shown great promise for the application as gas adsorbents, smart photonic devices, and photocatalysis.[2a,13] Its potential as high-performance separation membranes, however, has not been fully explored yet. As a new member of the titanium-oxo cluster family, $Ti_8O_8(OOCR)_{16}$ [$R = C_6H_5$] (Ti_8Ph), which consists of eight [TiO_6] octahedra in a ring linked by six μ_2- and two μ_3-O bridges,[14] possesses a similar structure to the $Ti_8(\mu_2\text{-}O)_8(\mu_2\text{-}OH)_4$ node in the MIL-125 framework, thereby making it an attractive alternative to common titanium sources. Additionally, our recent study indicated that compared with conventional heating methods, using single-mode microwave heating enabled better control of the microstructure of NH_2-MIL-125 (Ti) membranes, owing to a higher microwave field intensity and uniformity.[5] In the present work, with Ti_8Ph cluster as titanium source, highly defective MIL-125 membrane was prepared through combing single-mode microwave heating with tertiary growth (Figure 1). On the one hand, our research indicated that carrying out the reaction at lower temperatures enabled increasing missing-linker defects within MIL-125 framework, which warranted high-affinity interactions with CO_2 molecules at room temperature, thereby leading to high adsorption selectivity (14.3) as evidenced by the IAST model; on the other hand, relatively large pore size of MIL-125 warranted high diffusivity of smaller-sized gases through the membrane. As a result, not only the ideal CO_2/N_2 selectivity ranked the highest among all polycrystalline MOF membranes measured under similar conditions, but also the Robeson Upper Bound 2008 was overcome for versatile gas pairs. Most importantly, we found that only by using the Ti_8Ph cluster source could high-performance MIL-125 membranes be prepared. It is expected that this metal-oxo cluster-based protocol could bring

Figure 1. Schematic illustration of the preparation of the defective MIL-125 membrane with a Ti_8Ph cluster source through combing single-mode microwave heating with tertiary growth (BA: benzoic acid; BDC: terephthalic acid).

new insights into diverse high-performance MOF membrane preparations.

Results and Discussion

Our first step involves the synthesis of the Ti_8Ph cluster according to a previous procedure with a slight modification.[14] Relevant SEM images indicated that the obtained products exhibited a well-defined needle shape (Figure 2a). The corresponding XRD pattern coincided well with that of the standard Ti_8Ph phase, implying that a pure Ti_8Ph cluster phase had been formed (Figure 2b).

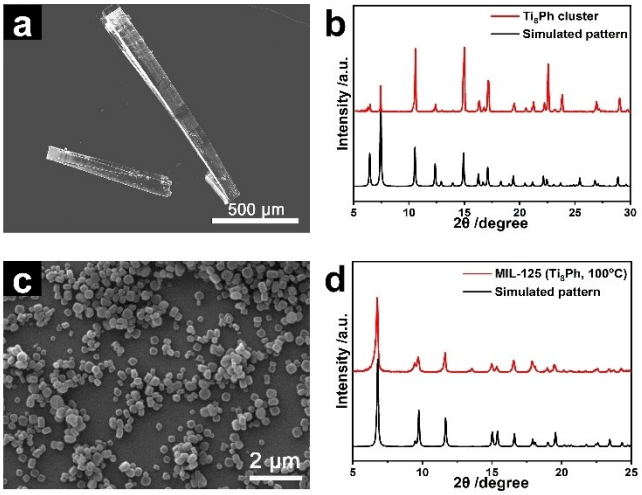

Figure 2. a) SEM image of the Ti_8Ph cluster. b) XRD patterns of the prepared Ti_8Ph cluster and simulated Ti_8Ph cluster. c) SEM image of MIL-125. d) XRD patterns of prepared MIL-125 (Ti_8Ph, 100 °C) and simulated MIL-125.

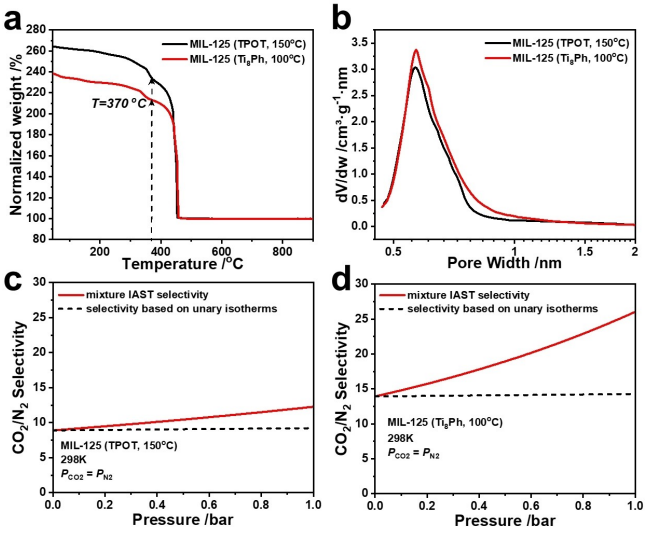

Figure 3. a) TG curves of MIL-125 (TPOT, 150 °C) and MIL-125 (Ti_8Ph, 100 °C). b) Pore size distributions of the above samples based on the H–K model. IAST selectivities for mixtures ($V_{CO_2}:V_{N_2}=50:50$, 0–1 bar) and unary selectivities of c) MIL-125 (TPOT, 150 °C) and d) MIL-125 (Ti_8Ph, 100 °C).

Subsequently, two kinds of MIL-125 powders were prepared using the Ti_8Ph cluster and TPOT as titanium sources, respectively. Our results indicated that uniform MIL-125 powders with an average size of 240 nm (Figure 2c,d and Figure S1) could be obtained by conducting a linker exchange reaction between Ti_8Ph clusters and BDC linkers at a temperature as low as 100 °C (denoted as MIL-125 (Ti_8Ph, 100 °C)). In contrast, the threshold temperature required for full conversion of TPOT to MIL-125 was 150 °C (denoted as MIL-125 (TPOT, 150 °C)) (Figure S2), indicating that using the Ti_8Ph cluster source significantly lowered the activation energy required for MIL-125 formation.

Considering the potential impact of missing-linker defects on the separation performance of MIL-125 membranes, herein the missing-linker number, which was widely used for quantitative evaluation of missing-linker defects, of the MIL-125 powders was determined by TG analysis (shown in Figure 3a). According to the method proposed by Lillerud et al.,[15] the missing-linker number per $Ti_8(\mu_2\text{-}O)_8(\mu_2\text{-}OH)_4$ node in the framework of MIL-125 (Ti_8Ph, 100 °C) reached 2.2, which was 5.5 times higher than that in MIL-125 (TPOT, 150 °C), implying that employing the Ti_8Ph cluster source resulted in a significant increase in missing-linker number. In the next step, textural properties of the above MIL-125 powders were studied further. As shown in Figure S3a, N_2 adsorption/desorption isotherms revealed that MIL-125 (Ti_8Ph, 100 °C) exhibited a typical type I isotherm with a BET surface area of 1453 m^2g^{-1}, a pore volume of 0.69 cm^3g^{-1}, and a pore size centering at 0.63 nm, which were all considerably higher than those of MIL-125 (TPOT, 150 °C) (1286.6 m^2g^{-1}, 0.60 cm^3g^{-1}, and 0.62 nm, respectively). Moreover, the CO_2 adsorption capacity of MIL-125 (Ti_8Ph, 100 °C) (103.42 m^3g^{-1}) measured under ambient conditions was much higher than that of MIL-125 (TPOT, 150 °C) (53.05 m^3g^{-1}), while maintaining similar N_2 adsorption capacity (Figure S3b). Much higher adsorption capacity of CO_2 than that of N_2 can be attributed to preferential adsorption of CO_2 on coordinatively unsaturated open metal sites in the MIL-125 framework.[16] Moreover, CO_2/N_2 ideal adsorbed solution theory (IAST) selectivity of the above MIL-125 powders was calculated according to CO_2 and N_2 adsorption isotherms under ambient conditions (Figure 3c,d). CO_2/N_2 ($V_{CO_2}:V_{N_2}=50:50$, 0–1 Bar) IAST selectivity of MIL-125 (Ti_8Ph, 100 °C) (32.2) was around three times higher than that of MIL-125 (TPOT, 150 °C) (11.4), implying that both CO_2 adsorption capacity and CO_2/N_2 adsorption selectivity were positively associated with the missing-linker number in MIL-125 framework, which coincided well with previous research.[17] The fitting curves of CO_2 and N_2 based on the original experimental adsorption data were shown in Figure S4, demonstrating that the fitting results of the two molecules are of good accuracy. We therefore concluded that possessing higher missing-linker number in the framework was in favor of enhancing the CO_2/N_2 separation performance of MIL-125 membranes. Moreover, the unary IAST selectivity was plotted by dashed lines in Figure 3c,d, calculated based

on the unary isotherms (Figure S3b), using the partial pressures in the mixture to calculate the loadings. The ratio of the CO_2/N_2 mixture IAST selectivity to unary IAST selectivity for MIL-125 (Ti_8Ph, 100 °C) and MIL-125 (TPOT, 150 °C) were 1.8 and 1.3 at 100 kPa, respectively. In addition, the MIL-125 pore occupancies at 1 bar were less than 10 %, therefore, the differences in the IAST selectivity for mixtures and unary selectivity are not large.

Considering the potential impact of the temperature on the missing-linker number in the MIL-125 framework, herein MIL-125 powders were further synthesized at higher temperatures (120 °C, 140 °C, and 160 °C) using the Ti8Ph cluster source. TG results (Figure S5) indicated that missing-linker numbers in the MIL-125 framework decreased sharply with increasing temperature, resulting in a decrease of both the CO_2 adsorption capacity and CO_2/N_2 adsorption selectivity (Figure S6). Moreover, the isosteric heats ($\approx$21.5 kJ mol^{-1}) of MIL-125 (Ti_8Ph, 100 °C) were calculated according to the CO_2 adsorption isosteres in a temperature range from 298 to 363 K (Figure S7) via the Clausius–Clapeyron equation, which was within the results previously reported in the literature.[18] Therefore, MIL-125 (Ti8Ph, 100 °C), which exhibited the highest missing-linker number and therefore, the highest CO_2 adsorption capacity and CO_2/N_2 adsorption selectivity, were chosen as seeds for the MIL-125 membrane preparation.

Subsequently, the spin-coating technique was employed to deposit MIL-125 (Ti_8Ph, 100 °C) on the porous α-Al_2O_3 substrate. As shown in Figure 4a, b, after spin-coating under optimized conditions, a uniform seed layer with thickness of 1.4 μm was obtained. Corresponding XRD pattern indicated that prepared MIL-125 seed layer was preferentially (00l)-oriented.

In the next step, secondary growth was carried out to seal intergranular gaps in the MIL-125 seed layer, during which the Ti_8Ph cluster was served as titanium source and the temperature was kept at 100 °C for maximizing the missing-linker number in the membrane. Relevant SEM images and EDXS pattern (Figure 4c–e) indicated that after single-mode microwave heating at 100 °C for 70 min, a well-intergrown MIL-125 membrane with thickness of 1.7 μm was obtained (denoted as MIL-125-SG). The corresponding

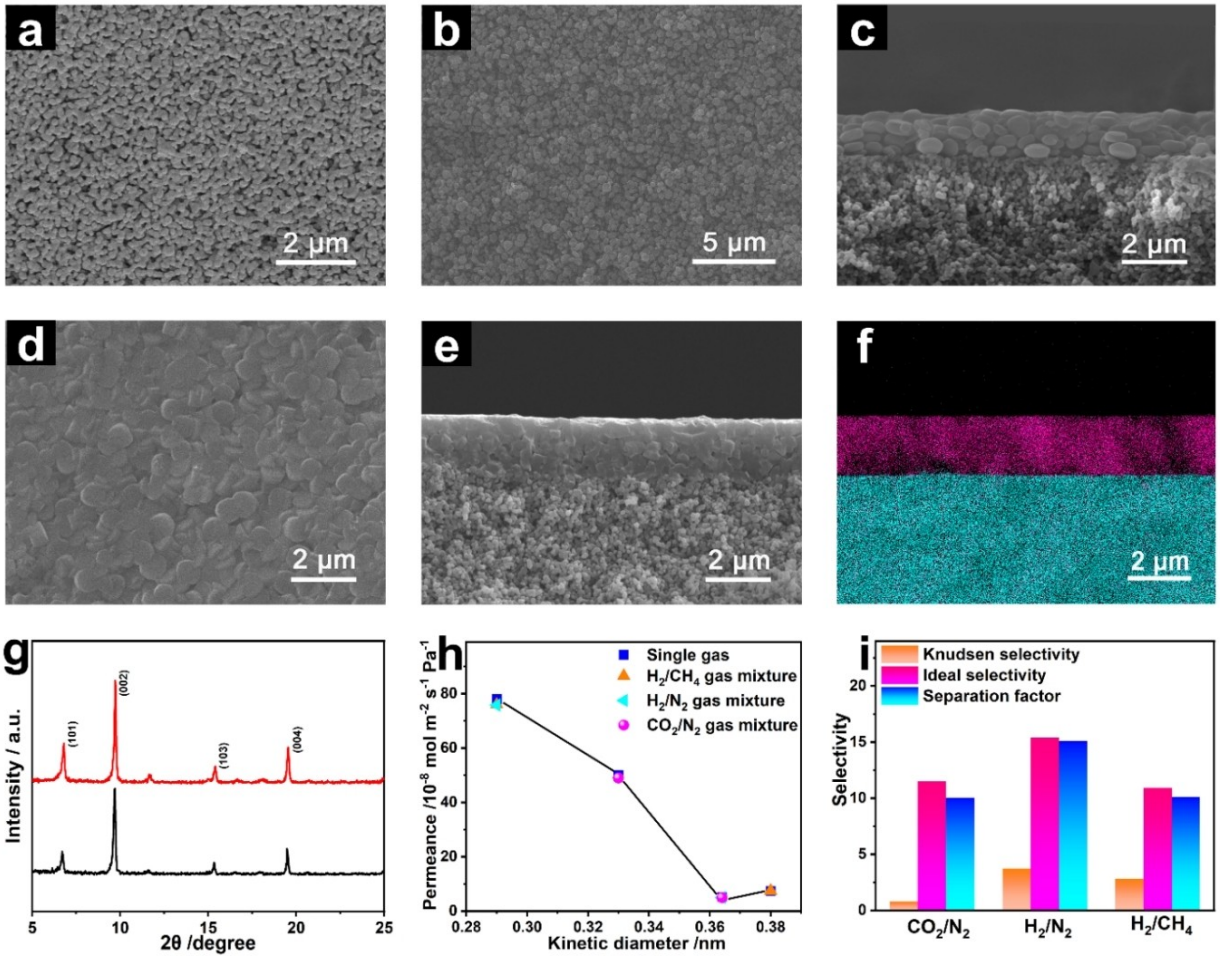

Figure 4. a) Top SEM image of porous α-Al_2O_3 substrate. Top and cross-sectional SEM images of b), c) MIL-125 seed layer and d), e) MIL-125-SG. f) Cross-sectional EDXS mapping of MIL-125-SG (color code: Ti = red; Al = blue). g) XRD patterns of MIL-125 seed layer (black line) and MIL-125-SG (red line). h) Single-gas and mixed-gas permeation properties of MIL-125-SG under ambient conditions. i) The Knudsen selectivity, ideal selectivity and SF of CO_2/N_2, H_2/N_2, and H_2/CH_4 gas pairs on MIL-125-SG.

XRD pattern (Figure 4f) confirmed that the prepared MIL-125-SG remained preferentially (00l)-oriented. Measurement equipment for single and mixed gas permeation is shown in Figure S8. Gas permeation results (Figure 4g,h and Table S1) indicated that ideal CO_2/N_2, H_2/N_2 and H_2/CH_4 selectivity of the MIL-125-SG reached 11.5, 15.4 and 10.9, respectively, which was much higher than the corresponding Knudsen selectivity (0.8, 3.74 and 2.83, respectively), thereby confirming the existence of few grain boundary defects in the membrane. In addition, prepared membrane maintained high H_2 permeance of 7.8×10^{-7} mol m^{-2} s^{-1} Pa^{-1}.

Afterwards, tertiary growth was carried out to further eliminate grain boundary defects in the membrane. Relevant SEM images (Figure 5a,b) showed that prepared MIL-125 membrane (denoted as MIL-125-TG) remained well-inter-

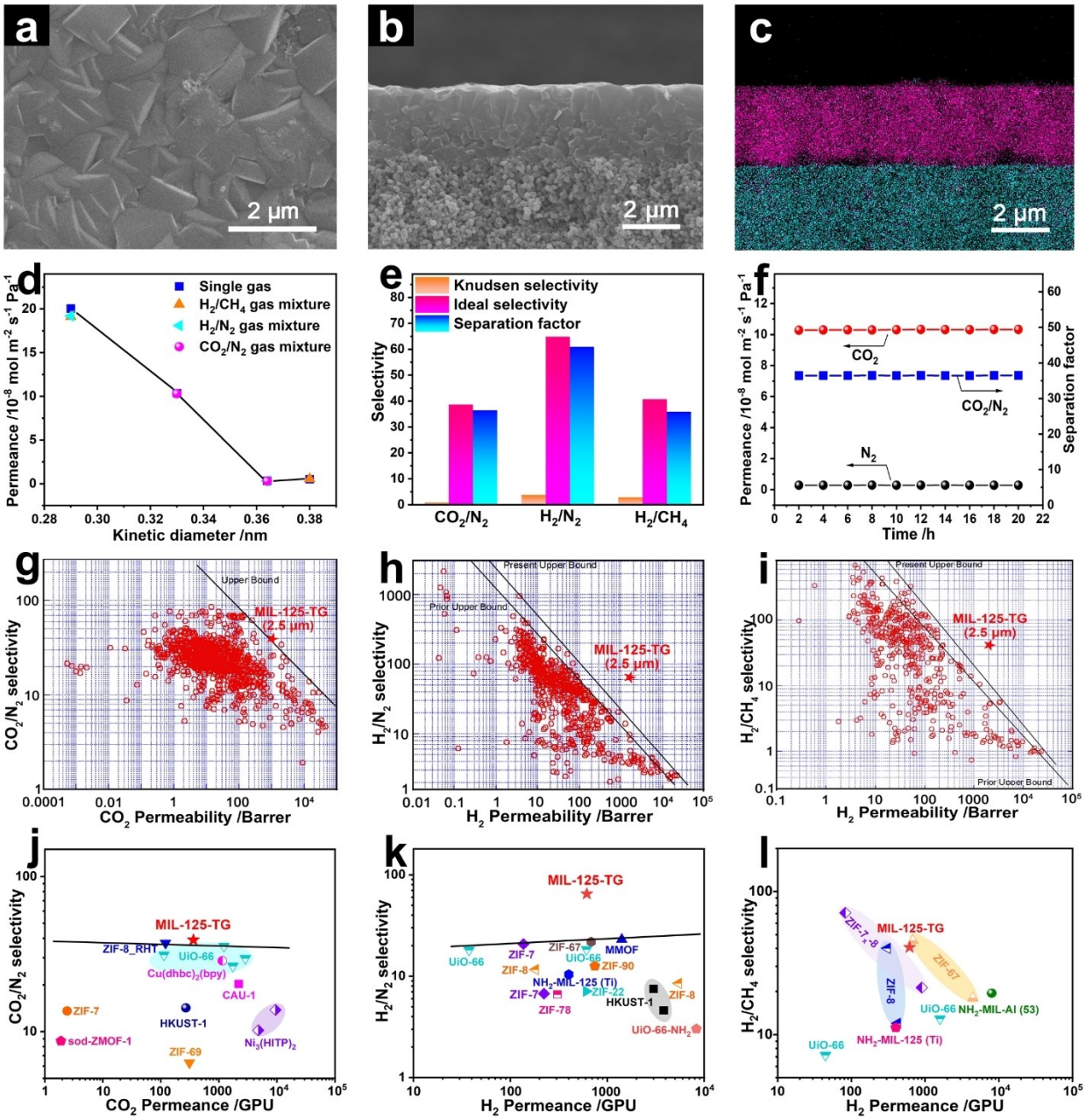

Figure 5. a) Top and b) cross-sectional SEM images of MIL-125-TG. c) Cross-sectional EDXS mapping of MIL-125-TG (color code: Ti = red; Al = blue). d) Single-gas and mixed-gas permeation properties of MIL-125-TG under ambient conditions. e) The Knudsen selectivity, ideal selectivity and SF of CO_2/N_2, H_2/N_2 and H_2/CH_4 gas pairs through MIL-125-TG. f) Long-term stability of MIL-125-TG under ambient conditions. Comparison of g) CO_2/N_2, h) H_2/N_2 and i) H_2/CH_4 separation performances of MIL-125-TG with their respective 2008 Robeson upper bounds. j) Comparison of CO_2/N_2 separation performance of MIL-125-TG with pristine MOF membranes measured under comparable conditions. Comparison of k) H_2/N_2 and l) H_2/CH_4 separation performance of MIL-125-TG with pristine 3D MOF membranes measured under comparable conditions. Detailed data are listed in Table S3–S5.

grown while the thickness was increased to 2.5 μm. Simultaneously, a clear boundary between the MIL-125 top layer and underlying porous α-Al_2O_3 substrate existed in the cross-sectional EDXS pattern (Figure 5c), indicating that the formed MIL-125 top layer did not penetrate deep into porous α-Al_2O_3 substrate pores, which was beneficial for reducing the diffusion barrier. Corresponding XRD pattern (Figure S9) indicated that prepared MIL-125-TG remained preferentially (00l)-oriented. The dye molecule rejection test was conducted to evaluate whether the grain boundaries are indeed further removed after the tertiary growth. Since the molecular size of Congo red (CR) dyes (2.53×0.73 nm) is larger than the pore size of MIL-125 but smaller than that of the grain boundary defects,[19] the CR rejection rate could be a true reflection of the grain boundary defect structure of the corresponding MIL-125 membrane. The dye rejection test results as shown in Figure S10 indicated that the CR rejection rate of MIL-125-TG reached 99.53 %, which was higher than that of MIL-125-SG (98.48 %), which vividly confirmed that majority of grain boundaries were removed after the tertiary growth.

Gas permeation results (Figure 5d, e and Table S2) indicated that ideal CO_2/N_2, H_2/N_2 and H_2/CH_4 selectivity of prepared MIL-125-TG sharply increased to 38.7, 64.9 and 40.7, respectively, making the overall separation performance well exceed their respective Robeson 2008 upper bound lines (Figure 5g–i).[20] Moreover, according to the sorption–diffusion model, the permeation selectivity (S_{perm}) may be expressed as the product of the adsorption and diffusion selectivity: $S_{perm} = S_{ads} \times S_{diff}$. Since S_{ads} of the CO_2/N_2 gas pair reached 14.3 (based on the IAST theory), correspondingly, the S_{diff} was calculated to be 2.7. Therefore, the excellent CO_2/N_2 separation performance of the MIL-125-TG could be mainly attributed to the high CO_2/N_2 adsorption selectivity.

We further investigated long-term stability of prepared MIL-125-TG (Figure 5f). After continuous operation over 20 h, both CO_2 permeance and separation factor (SF) of CO_2/N_2 remained unchanged, which was indicative of excellent operation stability. In particular, the ideal CO_2/N_2 selectivity of the MIL-125-TG was the highest among all pristine polycrystalline MOF membranes (Figure 5j and Table S3) measured under comparable conditions.[9,20,21] It should be noted that besides the CO_2/N_2 gas pair, MIL-125-TG membrane also exhibited excellent H_2/N_2 and H_2/CH_4 selectivity. In effect, many literatures have reported microporous materials with relatively large pores but enhancing H_2/N_2 or H_2/CH_4 separations. For instance, Liu et al. prepared well-intergrown, highly c-oriented ultrathin 2D Cu-TCPP (≈5.4 Å) membranes on porous α-Al_2O_3 substrates, which displayed H2/CH4 selectivity of ≈50;[22] Zhu et al. synthesized large pore (7.5 Å) NH_2-MIL-53 (Al) membranes displaying high SF for H_2/N_2 (23.9) and H_2/CH_4 (20.7) gas mixtures, respectively;[23] Li et al. fabricated UiO-66 (≈6.0 Å) membranes with high H_2/N_2 SF (22.4);[21c] Pinnau et al. prepared AB-type ladder TPIM-1 (≈5.5 Å) membranes with high selectivity for H_2/N_2 (≈50) and H_2/CH_4 (≈53) gas pairs;[24] Cooper et al. synthesized porous organic cage (≈5.8 Å) membranes displaying the H_2/N_2 selectivity as high as 33.[25] It was highly possible that the unique framework topology of MIL-125 contributed to enhanced H_2/N_2 and H_2/CH_4 separations. In addition, the preferred c-orientation, the low reaction temperature, and the conduction of tertiary growth were beneficial for reducing grain boundary defects and therefore, enhancing H_2/N_2 and H_2/CH_4 separations of prepared MIL-125 membranes. The ideal H_2/N_2 and H_2/CH_4 selectivity was also superior to those obtained with most pristine polycrystalline MOF membranes reported in the literature (Figure 5k,l and Table S4, S5), thereby showing a versatile utility for efficient gas separation on diverse occasions.

Considering its potential applications in industrial separation of CO_2 from flue gases, the CO_2/N_2 separation performance of prepared MIL-125-TG was further studied by simulating the composition of flue gases ($V_{CO_2}:V_{N_2} = 15:85$). Gas permeation results indicated that both CO_2 permeance and CO_2/N_2 SF remained largely unchanged (1.1×10^{-7} mol m^{-2} s^{-1} Pa^{-1} and 35.9, respectively), which was in sharp contrast to other CO_2-permselective MOF (e.g., UiO-66 and CAU-1) membranes whose CO_2/N_2 selectivity sharply decreased with decreasing CO_2/N_2 ratio on the feed side[21g,h] and therefore, quite advantageous for stable operation under varying working conditions.

Finally, the effect of operating temperature on the CO_2/N_2 separation performance of prepared MIL-125-TG was investigated. As shown in Figure S11, the CO_2 permeance first increased with the elevation of temperature and reached maximum value at 90 °C, while further increasing the temperature led to decreased CO_2 permeance. In contrast, the N_2 permeance steadily increased upon elevating temperature, resulting in a steady decrease in SF of CO_2/N_2. To study CO_2 permeation kinetics in the MIL-125 framework in detail, the sorption-diffusion model was employed to investigate the variation trend of adsorption coefficient (S_i) and diffusion coefficient (D_i) for CO_2. The plots of P_{CO_2}, D_{CO_2}, and S_{CO_2} against temperature were shown in Figure S12, which preliminarily proved that CO_2 permeation process was dominantly controlled by diffusion in the case that the temperature was lower than 363 K, while it became adsorption-controlled when the temperature became higher than 363 K. Furthermore, we calculated the activation energies of permeability (E_p), heats of adsorption (negative enthalpy of adsorption: $-\Delta H$) and activation energies of diffusion (E_D) for CO_2 (Table S6) based on the Arrhenius plots for the permeability, S_{CO_2} and D_{CO_2} in the temperature ranges of 303 to 333 K, 333 to 363 K, 363 to 393 K, and 393 to 423 K (Figure S13). To summarize, the above results vividly confirmed that the CO_2 permeability was mainly controlled by diffusion at 303–363 K, while adsorption played a dominant role at 363–423 K.

Considering the potential impact of the titanium source on the separation performance of MIL-125 membranes, as a comparative experiment, MIL-125 membranes were further prepared by using 240 nm-sized MIL-125 (TPOT, 150 °C) (Figure S14a) as seeds and TPOT as the titanium source during membrane growth while keeping other synthetic conditions unchanged. Our experimental results indicated that even after tertiary growth at 100 °C for 70 min, prepared

MIL-125 membrane remained poorly intergrown (Figure S14b–e), which might be attributed to relatively high activation energy required for the $Ti_8(\mu_2\text{-}O)_8(\mu_2\text{-}OH)_4$ node formation before the membrane growth. As a result, elevating the temperature to 160 °C was indispensable for the well intergrowth between adjacent MIL-125 crystallites (Figure S15).[5,26] Gas permeation results indicated that ideal CO_2/N_2, H_2/N_2 and H_2/CH_4 selectivity of the MIL-125 membrane synthesized at 160 °C was only 5.3, 7.0 and 1.5 (Table S7 and S8), which could be ascribed to relatively low missing-linker number (~0.4) in the membrane, resulting in lower CO_2/N_2 adsorption selectivity and therefore, inferior CO_2/N_2 separation performance.

To investigate the impact of heating mode on the separation performance, MIL-125 membranes were further prepared by convective heating for comparison. As shown in Figure S16, substantial voids and cracks remained visible in the membrane even after prolonged growth (24 h). Simultaneously, we observed that substantial MIL-125 particles (mass: 90 mg, yield: 92 %) were spontaneously formed and sedimented to the bottom of the vessel after the reaction (Figure S17). Accordingly, failure of well-intergrown MIL-125 membrane formation could be ascribed to excessive MIL-125 nucleation and growth in the bulk solution, resulting in over-consumption of nutrients there and therefore, inadequate nutrient supply for sealing intergranular gaps in the membrane. In contrast, owing to the nucleation bottleneck effect, only a small amount of amorphous powders was generated in the bulk solution in the case of single-mode microwave heating, resulting in effective suppression of MIL-125 nucleation in the bulk solution and therefore, sufficient nutrient supply for the formation of well-intergrown MIL-125 membranes.[5,26]

To investigate the influence of reaction temperature on the separation performance, MIL-125 membranes were further prepared at 160 °C with Ti_8Ph cluster source while keeping other reaction conditions unchanged. SEM results (Figure S18) indicated that after tertiary growth, a well-intergrown, 3.8 μm-thick MIL-125 membrane was obtained. Gas permeation results indicated that ideal CO_2/N_2, H_2/N_2 and H_2/CH_4 selectivity of the membrane was 9.0, 8.3 and 5.2, respectively (Table S9). The relatively low selectivity could be attributed to effective elimination of missing-linker defects (missing-linker number: 0) in the framework at such a high temperature, resulting in lower CO_2/N_2 adsorption selectivity.

Conclusion

With the Ti_8Ph cluster as titanium source, a highly defective MIL-125 membrane was successfully fabricated through combining single-mode microwave heating with tertiary growth in this study. Employing the Ti_8Ph cluster source led to not only a lower reaction temperature required for the formation of a well-intergrown MIL-125 membrane but also a higher missing-linker number within the framework, resulting in enhanced CO_2/N_2 adsorption selectivity. The prepared MIL-125 membrane exhibited an ideal CO_2/N_2 selectivity of 38.7, which ranked the highest among all pristine polycrystalline MOF membranes measured under similar conditions. Of particular note, a simulated flue gas separation experiment indicated that both CO_2 permeance and CO_2/N_2 SF (35.9) remained unchanged, which was in sharp contrast to other CO_2-permselective MOF membranes whose CO_2/N_2 selectivity sharply decreased with decreasing CO_2/N_2 ratio on the feed side, which was quite advantageous for stable operation under varying working conditions. In addition, its ideal H_2/N_2 and H_2/CH_4 selectivity (64.9 and 40.7) were notably high. It is anticipated that the concept of using metal-oxo clusters as metal sources could bring new insights into diverse high-performance MOF membrane preparations.

Acknowledgements

We are grateful to National Natural Science Foundation of China (22078039, 21922810), Science and Technology Innovation Fund of Dalian (2020JJ26GX026), Fok Ying-Tong Education Foundation of China (171063), Science Fund for Creative Research Groups of the National Natural Science Foundation of China (22021005), National Key Research and Development Program of China (2019YFE0119200), and the Technology Innovation Team of Dalian University of Technology (DUT2017TB01) for the financial support.

Conflict of Interest

The authors declare no conflict of interest.

Data Availability Statement

Research data are not shared.

Keywords: Gas Separation · Membranes · Metal–Organic Frameworks · Structural Defects · Ti-Oxo Clusters

[1] S. Hong, Y. Jeong, H. Baik, N. Choi, A. C. K. Yip, J. Choi, *Angew. Chem. Int. Ed.* **2021**, *60*, 1323–1331; *Angew. Chem.* **2021**, *133*, 1343–1351.
[2] a) M. Dan-Hardi, C. Serre, T. Frot, L. Rozes, G. Maurin, C. Sanchez, G. Férey, *J. Am. Chem. Soc.* **2009**, *131*, 10857–10859; b) S. Yang, L. Peng, S. Bulut, W. L. Queen, *Chem. Eur. J.* **2019**, *25*, 2161–2178.
[3] a) Y. Sun, D.-F. Lu, Y. Sun, M.-Y. Gao, N. Zheng, C. Gu, F. Wang, J. Zhang, *ACS Mater. Lett.* **2021**, *3*, 64–68; b) P. Ji, Y. Song, T. Drake, S. S. Veroneau, Z. Lin, X. Pan, W. Lin, *J. Am. Chem. Soc.* **2018**, *140*, 433–440.
[4] S. Friebe, A. Mundstock, D. Unruh, F. Renz, J. Caro, *J. Membr. Sci.* **2016**, *516*, 185–193.
[5] Y. Sun, Y. Liu, J. Caro, X. Guo, C. Song, Y. Liu, *Angew. Chem. Int. Ed.* **2018**, *57*, 16088–16093; *Angew. Chem.* **2018**, *130*, 16320–16325.
[6] H. Assi, G. Mouchaham, N. Steunou, T. Devic, C. Serre, *Chem. Soc. Rev.* **2017**, *46*, 3431–3452.

[7] Z. Qiao, Y. Liang, Z. Zhang, D. Mei, Z. Wang, M. D. Guiver, C. Zhong, *Adv. Mater.* **2020**, *32*, 2002165.
[8] T. H. Lee, J. G. Jung, Y. J. Kim, J. S. Roh, H. W. Yoon, B. S. Ghanem, H. W. Kim, Y. H. Cho, I. Pinnau, H. B. Park, *Angew. Chem. Int. Ed.* **2021**, *60*, 13081–13088; *Angew. Chem.* **2021**, *133*, 13191–13198.
[9] J. Yan, Y. Sun, T. Ji, L. Liu, M. Zhang, Y. Liu, *J. Membr. Sci.* **2021**, *635*, 119515.
[10] a) V. Guillerm, S. Gross, C. Serre, T. Devic, M. Bauer, G. Ferey, *Chem. Commun.* **2010**, *46*, 767–769; b) D. C. Oliveira, A. G. Macedo, N. J. O. Silva, C. Molina, R. A. S. Ferreira, P. S. Andre, K. Dahmouche, V. D. Z. Bermudez, Y. Messaddeq, S. J. L. Ribeiro, L. D. Carlos, *Chem. Mater.* **2008**, *20*, 3696–3705.
[11] Y. Keum, S. Park, Y.-P. Chen, J. Park, *Angew. Chem. Int. Ed.* **2018**, *57*, 14852–14856; *Angew. Chem.* **2018**, *130*, 15068–15072.
[12] S. Wang, H. Reinsch, N. Heymans, M. Wahiduzzaman, C. Martineau-Corcos, G. De Weireld, G. Maurin, C. Serre, *Matter* **2020**, *2*, 440–450.
[13] S. Hu, M. Liu, X. Guo, K. Li, Y. Han, C. Song, G. Zhang, *Cryst. Growth Des.* **2017**, *17*, 6586–6595.
[14] T. Frot, S. Cochet, G. Laurent, C. Sassoye, M. Popall, C. Sanchez, L. Rozes, *Eur. J. Inorg. Chem.* **2010**, 5650–5659.
[15] G. C. Shearer, S. Chavan, S. Bordiga, S. Svelle, U. Olsbye, K. P. Lillerud, *Chem. Mater.* **2016**, *28*, 3749–3761.
[16] Ü. Kökçam-Demir, A. Goldman, L. Esrafili, M. Gharib, A. Morsali, O. Weingart, C. Janiak, *Chem. Soc. Rev.* **2020**, *49*, 2751–2798.
[17] J. N. Hall, P. Bollini, *React. Chem. Eng.* **2019**, *4*, 207–222.
[18] S.-N. Kim, J. Kim, H.-Y. Kim, H.-Y. Cho, W.-S. Ahn, *Catal. Today* **2013**, *204*, 85–93.
[19] S. Hong, D. Kim, H. Richter, J.-H. Moon, N. Choi, J. Nam, J. Choi, *J. Membr. Sci.* **2019**, *569*, 91–103.
[20] L. M. Robeson, *J. Membr. Sci.* **2008**, *320*, 390–400.
[21] a) B. A. Al-Maythalony, O. Shekhah, R. Swaidan, Y. Belmabkhout, I. Pinnau, M. Eddaoudi, *J. Am. Chem. Soc.* **2015**, *137*, 1754–1757; b) D. S. Chiou, H. J. Yu, T. H. Hung, Q. Lyu, C. K. Chang, J. S. Lee, L. C. Lin, D. Y. Kang, *Adv. Funct. Mater.* **2021**, *31*, 2006924; c) X. Liu, N. K. Demir, Z. Wu, K. Li, *J. Am. Chem. Soc.* **2015**, *137*, 6999–7002; d) Y. Liu, G. Zeng, Y. Pan, Z. Lai, *J. Membr. Sci.* **2011**, *379*, 46–51; e) R. Rong, Y. Sun, T. Ji, Y. Liu, *J. Membr. Sci.* **2020**, *610*, 118275; f) M. N. Shah, M. A. Gonzalez, M. C. McCarthy, H.-K. Jeong, *Langmuir* **2013**, *29*, 7896–7902; g) W. Wu, Z. Li, Y. Chen, W. Li, *Environ. Sci. Technol.* **2019**, *53*, 3764–3772; h) H. Yin, J. Wang, Z. Xie, J. Yang, J. Bai, J. Lu, Y. Zhang, D. Yin, J. Y. Lin, *Chem. Commun.* **2014**, *50*, 3699–3701; i) R. W. Baker, B. T. Low, *Macromolecules* **2014**, *47*, 6999–7013; j) M. Galizia, W. S. Chi, Z. P. Smith, T. C. Merkel, R. W. Baker, B. D. Freeman, *Macromolecules* **2017**, *50*, 7809–7843; k) T. H. Lee, A. Ozcan, I. Park, D. Fan, J. K. Jang, P. G. M. Mileo, S. Y. Yoo, J. S. Roh, J. H. Kang, B. K. Lee, Y. H. Cho, R. Semino, H. W. Kim, G. Maurin, H. B. Park, *Adv. Funct. Mater.* **2021**, *31*, 2103973; l) U. W. R. Siagian, A. Raksajati, N. F. Himma, K. Khoiruddin, I. G. Wenten, *J. Nat. Gas Sci. Eng.* **2019**, *67*, 172–195; m) Y. Wang, H. Jin, Q. Ma, K. Mo, H. Mao, A. Feldhoff, X. Cao, Y. Li, F. Pan, Z. Jiang, *Angew. Chem. Int. Ed.* **2020**, *59*, 4365–4369; *Angew. Chem.* **2020**, *132*, 4395–4399; n) S. Jiang, X. Shi, F. Sun, G. Zhu, *Chem. Asian J.* **2020**, *15*, 2371–2378; o) S. Jiang, X. Shi, Y. Zu, F. Sun, G. Zhu, *Mater. Chem. Front.* **2021**, *5*, 5150–5157; p) Y. Ying, Z. Zhang, S. B. Peh, A. Karmakar, Y. Cheng, J. Zhang, L. Xi, C. Boothroyd, Y. M. Lam, C. Zhong, D. Zhao, *Angew. Chem. Int. Ed.* **2021**, *60*, 11318–11325; *Angew. Chem.* **2021**, *133*, 11419–11426.
[22] Y. Song, Y. Sun, D. Du, M. Zhang, Y. Liu, L. Liu, T. Ji, G. He, Y. Liu, *J. Membr. Sci.* **2021**, *634*, 119393.
[23] F. Zhang, X. Zou, X. Gao, S. Fan, F. Sun, H. Ren, G. Zhu, *Adv. Funct. Mater.* **2012**, *22*, 3583–3590.
[24] B. S. Ghanem, R. Swaidan, X. Ma, E. Litwiller, I. Pinnau, *Adv. Mater.* **2014**, *26*, 6696–6700.
[25] Q. Song, S. Jiang, T. Hasell, M. Liu, S. Sun, A. K. Cheetham, E. Sivaniah, A. I. Cooper, *Adv. Mater.* **2016**, *28*, 2629–2637.
[26] Y. Sun, C. Song, X. Guo, S. Hong, J. Choi, Y. Liu, *J. Membr. Sci.* **2020**, *616*, 118615.

Manuscript received: March 10, 2022
Accepted manuscript online: April 14, 2022
Version of record online: May 3, 2022

Angewandte Chemie
Eine Zeitschrift der Gesellschaft Deutscher Chemiker

Supporting Information

Titanium-Oxo Cluster Assisted Fabrication of a Defect-Rich Ti-MOF Membrane Showing Versatile Gas-Separation Performance

*C. Wang, Y. Sun, L. Li, R. Krishna, T. Ji, S. Chen, J. Yan, Y. Liu**

SUPPORTING INFORMATION

Table of Contents

1. Experimental Procedures

1.1 Materials

Titanium(IV) isopropoxide (TPOT, 99.9%, Macklin), benzoic acid (BEN, 99%, Aladdin), 1,4-dicarboxybenzene (BDC, 99%, Aladdin), methyl cyanide (MeCN, 99.5%, Kermel), N, N-dimethylformamide (DMF, 99.5%, Kermel), and methanol (MeOH, 99.5%, Kermel) were used as received without further purification. Porous α-Al_2O_3 disks with a pore size of 70 nm, diameter of 18 mm, and thickness of 1 mm were bought from Fraunhofer IKTS, Germany.

1.2 Synthesis of $Ti_8O_8(OOCC_6H_5)_{16}$ (Ti_8Ph cluster)

Ti_8Ph cluster was synthesized following a procedure developed by Rozes et al..[1] Briefly, 10.2 mL of MeCN containing 1.596 mL of TPOT was added to 51 mL of acetonitrile containing 5.617g of BEN. After ultrasonication for 30 min, obtained clear solution was transferred to a 100 mL Teflon-lined autoclave, and then solvothermal treated at 100 °C under static conditions for 15 h. After cooling to room temperature, needle-like precipitates, i.e., Ti_8Ph clusters, were obtained.

1.3 Synthesis of MIL-125 seeds

1.3.1 Synthesis of MIL-125 (Ti_8Ph, 100 °C)

0.84 g of BDC and 0.25 g of Ti_8Ph cluster were dissolved in a solution containing 27 mL of DMF and 3 mL of MeOH and then subjected to ultrasonic for 5 min. Subsequently, the mixture solution was transferred to a 50 mL Teflon-lined autoclave and solvothermal treated at 100 °C under static conditions for 24 h. After naturally cooling to room temperature, the resulting product was sequentially washed three times with DMF and MeOH, respectively, and finally dried overnight at 60 °C, the white powders of MIL-125 (Ti_8Ph, 100 °C) was obtained. To remove excess solvent molecules, MIL-125 (Ti_8Ph, 100 °C) powders were vacuum dried overnight at 200 °C.
In addition, other series of MIL-125 powders were prepared by the similar procedure of MIL-125 (Ti_8Ph, 100 °C) except that the heating temperature was 120, 140 and 160 °C, respectively.

1.3.2 Synthesis of MIL-125 (TPOT, 150 °C)

0.84 g of BDC, 0.3 mL of TPOT and p-toluylic acid were dissolved in a solution containing 27 mL of DMF and 3 mL of MeOH under ultrasonic for 5min. The mixture solution was transferred to a 50 mL Teflon-lined autoclave and solvothermal treated at 150 °C with static conditions for 24 h. After natural cooling, the resulting product was washed three times with DMF and methanol, respectively, and was dried overnight at 60 °C. To remove excess solvent molecules, MIL-125 (TPOT, 150 °C) powders were vacuum dried overnight at 200 °C.

In this work, all Ti-MOF powders were washed with DMF and MeOH solvents several times to remove residual titanium sources and ligands. After drying overnight at 60 °C, vacuum was further carried out at 200 °C overnight to remove majority of solvent molecules which remained trapped in the MIL-125 framework.

1.4 Deposition of MIL-125 seed layers

The seeds suspension was prepared by dispersing 0.05 g MIL-125 (Ti_8Ph, 100 °C) in 12.64 mL of methanol with stirring at room temperature for three days. The MIL-125 (Ti_8Ph, 100 °C) suspension was deposited on a α-Al_2O_3 plate by the spin-coated at 3,000 rpm for 60 s, followed by drying at room temperature for another 1 day and the MIL-125 seed layer was obtained.

1.5 Fabrication of MIL-125-SG

0.42 g of BDC and 0.125 g of Ti_8Ph cluster were dissolved in 30 mL of DMF-MeOH (v:v=1:1) binary solution under ultrasonication for 5min. Then the MIL-125 seed layer-modified porous α-Al_2O_3 substrate was vertically placed in an 80 mL glass vessel. After the addition of the above precursor solution, the vessel was sealed and heated at 100 °C for 70 min in a single-mode microwave oven (Discover, CEM). Finally, the vessel was sequentially fetched out, cooled to room temperature, rinsed with methanol, and dried overnight at room temperature, the MIL-125-SG was prepared.

In this work, our pretreatment condition for MOF membranes is the same as that of other Ti-MOF membranes. To further prove that the Ti_8Ph cluster source had been completely removed after the pretreatment, XRD characterization was carried out. The XRD result indicated that there existed no characteristic peak derived from Ti8Ph cluster in both MIL-125 powders and MIL-125 membranes, indicating that the Ti_8Ph cluster source had been fully removed.

1.6 Fabrication of MIL-125-TG

The procedure for the synthesis of MIL-125-TG was similar to that of MIL-125-SG except that MIL-125-SG was vertically placed in the above glass vessel instead.

1.7 Fabrication of MIL-125 membranes at 160 °C

The procedure for the preparation of the MIL-125 membrane was similar to that of MIL-125-TG except that both secondary growth and tertiary growth were conducted at 160 °C for 10 min instead.

1.8 Fabrication of MIL-125 membranes by solvothermal heating

The procedure for the preparation of the MIL-125 membrane was similar to that of MIL-125-TG except that both secondary growth and tertiary growth were conducted at 100 °C for 24 h in a convection oven instead.

1.9 Fabrication of MIL-125 membranes using TPOT source

The procedure for the preparation of the MIL-125 membrane was similar to that of MIL-125-TG except that 1) MIL-125 (TPOT, 150 °C) were used as seeds, 2) TPOT was used as titanium source during both secondary growth and tertiary growth, and 3) both secondary growth and tertiary growth were conducted at 160 °C for 10 min instead.

1.10 Characterization

XRD patterns were collected on Rigaku X-ray SmartLab diffractometer with Cu− Kα radiation in the range of 5–50° at a scanning rate of 8°·min^{-1} at 45 kV and 200 mA. SEM images were obtained on a Field-Emission Scanning Electron Microscope (NOVA NanoSEM 450). CO_2 and N_2 adsorption isotherms were recorded on Micromeritics ASAP 2020 Plus HD88. TG analysis was conducted on a NETZSCH (TG 209) thermal analyzer in air flux from 40 to 900 °C with a ramping rate of 10 K·min^{-1}.

2. Equation section

2.1 Calculation of gas adsorption selectivity by ideal adsorption solution theory (IAST)

Fitting adsorption isotherms to experimental data

The 1-site Langmuir-Freundlich isotherm model was adopted to fit the adsorption isotherms of CO_2 and N_2 on MIL-125 seeds at 298 K and 1 bar as follows:

$$q=q_{A,sat}\frac{b_A P^{v_A}}{1+b_A P^{v_A}}$$

with T-dependent parameters b_A

$$b_A=b_{AO}\,exp\left(\frac{E_A}{RT}\right)$$

where $\boldsymbol{q}$ represents the adsorption amount of adsorbents with units of mol/kg, $q_{A,sat}$ represent the saturated adsorption amount for adsorption sites A, $\boldsymbol{b_A}$ are constants for species i at adsorption sites A, $\boldsymbol{p}$ is the total pressure of the bulk gas at the adsorption equilibrium, and $\boldsymbol{v_A}$ is the Freundlich exponent for sites A.

2.2 Clausius−Clapeyron equation

The Clausius−Clapeyron equation is used to determine the isosteric heat of adsorption as a function of CO_2 loading:

$$-\Delta H = R_g T^2 (\frac{\partial lnP}{\partial T})_q$$

$$lnP = -\frac{-\Delta H}{R_g}\frac{1}{T} + A$$

Where R_g is the universal gas constant, T is the system temperature in Kelvin, and A is the integration constant. With a representation of ln$P$ (P, kPa) as a function of $1/T$ for CO_2, the corresponding isosteric heat of adsorption ($-\Delta H$) is obtained from the slope.

2.3 Gas permeation experiment details

For the single gas permeation measurement, the prepared MIL-125 (Ti) membrane was fixed in a module sealed with O-rings. The feed and sweep volumetric flow rate were both maintained at 50 ml·min^{-1} applied to the feed side of the membrane, and the permeated gas was removed by sweeping with sweep gas. Pressures at the feed side and permeate side were maintained at 1 bar. For the mixed gas permeation test, the feed flow rate was kept constant with a volumetric flow rate of 50 ml·min^{-1} for each gas, and the sweep flow rates were also set to 50 ml·min^{-1}, whereas the pressure at both sides was kept at 1 bar. The concentration of single/mixed gases on the permeate side was measured by the calibrated gas chromatography (7890B, Agilent).
The separation factor $\alpha_{i/j}$ is usually used to evaluate the target gas molecule separation performance of the membrane, which is defined as the quotient of the molar ratios of the components in the permeate side (y_i/y_j) divided by the quotient of the molar ratio of the components (x_i/x_j) in the feed side:

$$\alpha_{i/j} = \frac{y_i/x_i}{y_i/x_j}$$

The ideal selectivity $\alpha^*_{i/j}$ is defined as the single gas permeance ratio:

$$\alpha^*_{i/j} = \frac{P_i}{P_j}$$

Permeability (P_i) is defined as the product of permeance and membrane thickness (l). Barrer is the commonly used unit of Permeability:

$$P_i(permeability) = P_i(permeance) \times l$$

$$1\ Barrer = 10^{-10}\frac{cm^3(STP)cm}{cm^2 s\ cmHg}$$

Permeance (P_i) is defined as the the permeance per unit of transmembrane driving force (pressure difference). GPU is the commonly used unit of Permeance:

$$P_i(permeance) = \frac{J_i}{\Delta p} = \frac{cm^3(STP)}{cm^2 s\ cmHg}$$

$$1\ GPU = 10^{-6}\frac{cm^3(STP)}{cm^2 s\ cmHg}$$

2.4 Sorption-diffusion model

Diffusion coefficient (D_i, m^{2}s^{-1}) is defined as the kinetic transport across the membrane. Adsorption coefficient (S_i, cm^3(STP)cm^{-3} mmHg^{-1}) represents the thermodynamic affinity of the membrane material for one of the components in the feed mixture:

$$P_i = D_i \times S_i$$

2.5 The temperature dependence of permeability could be expressed by Arrhenius equation:

$$P_i = P_{i,0} exp\left(-\frac{E_p}{R_g T}\right)$$

Where E_p is the activation energy of permeability and $P_{i,0}$ is preexponential factor. E_p can also be expressed as follow:

$$E_P = \Delta H + E_D$$

Where ΔH is the enthalpy of adsorption and E_D is the activation energy of diffusion. Arrhenius equation can also be expressed as follows:

$$P_i = P_{i,0} exp\left(-\frac{\Delta H + E_D}{R_g T}\right)$$

2.6 Quantitative analysis of linker deficiency in MIL-125 powders

The number of linker deficiency can be calculated according to the reference as follows[2]:

$$x = 6 - \left(\frac{W_{Exp.plat} - W_{End}}{Wt.PL_{Theo}}\right)$$

x = Number of linker deficiency per Ti_8 formula unit
$W_{Exp.Plat}$ = Experimental TG plateau weight of defective $Ti_8O_{10}(BDC)_6$
W_{End} = Final weight of the TG run = Normalized to 100% (TiO_2)
$Wt.PL_{Theo}$ = Theoretical TG plateau weight of dehydroxylated $Ti_8O_{10}(BDC)_6$ without defects = 23.17%

2.7 Congo red (CR) dye rejection test

The amount of congo red dye aqueous solution (100 mg·L^{-1}) was added to the feed side and diffused in the permeate side. The aqueous solution permeation was driven by N_2 filled in the feed side with a pressure difference of 3 bar through the membrane. Meanwhile, a magnetic stirrer was used during the whole dye rejection test to alleviate the concentration polarization at the feed side. The rejection ***R*** (%) of dye is defined as following:

$$R = \frac{(C_f - C_P) \times 100}{C_f}$$

where C_f and C_p are the concentrations of corresponding dyes in the feed side and the permeate side, respectively.
The permeance ***P*** (L·m^{-2}·h^{-1}·bar^{-1}) of dye is defined as following:

$$P = \frac{V}{A \times t \times \Delta p}$$

Where ***V*** (L) is the volume of the permeate flowing across the membrane with an effective area ***A*** (m^2) within the time period ***t*** (h) at the operating transmembrane pressure Δ*p* (bar).

3 Results and Discussion

3.1 Supplementary Figures (Figure S1 to S18)

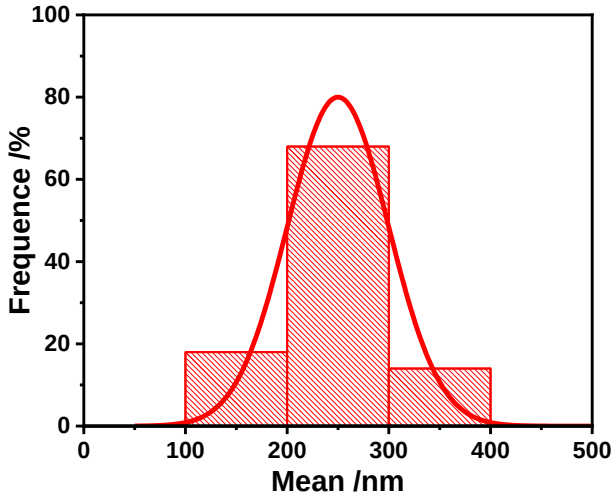

Figure S1. The size distribution of MIL-125 (Ti_8Ph, 100 °C).

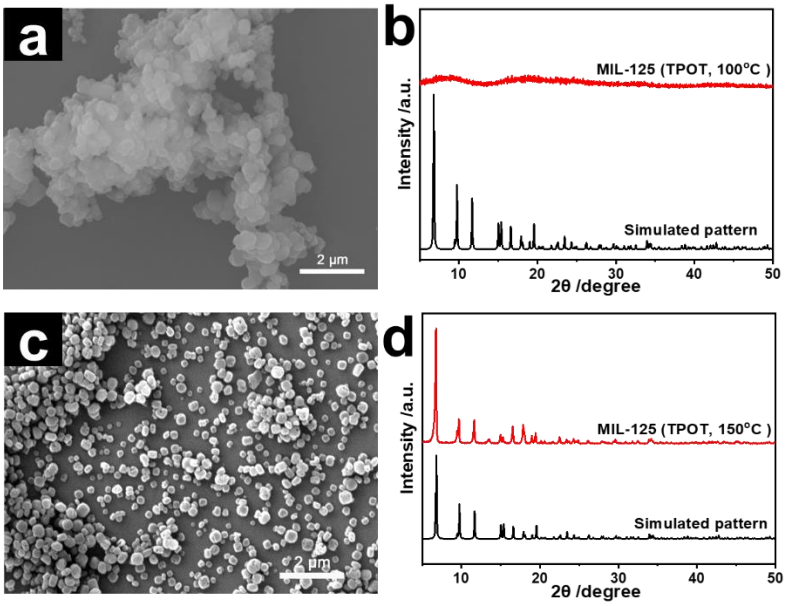

Figure S2. (a) SEM image and (b) XRD pattern of MIL-125 seeds synthesized using TPOT as Ti source at 100 °C for 24 h. (c) SEM image and (d) XRD pattern of MIL-125 seeds synthesized using TPOT as Ti source at 150 °C for 24 h.

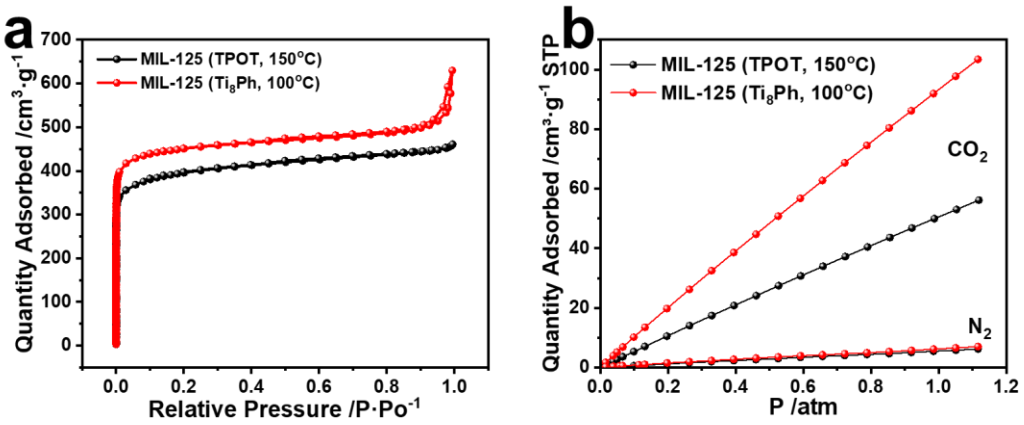

Figure S3. (a) N_2 adsorption of MIL-125 (TPOT, 150 °C) and MIL-125 (Ti_8Ph, 100 °C) at 77 K. (b) Corresponding CO_2 and N_2 adsorption isotherms at 298 K.

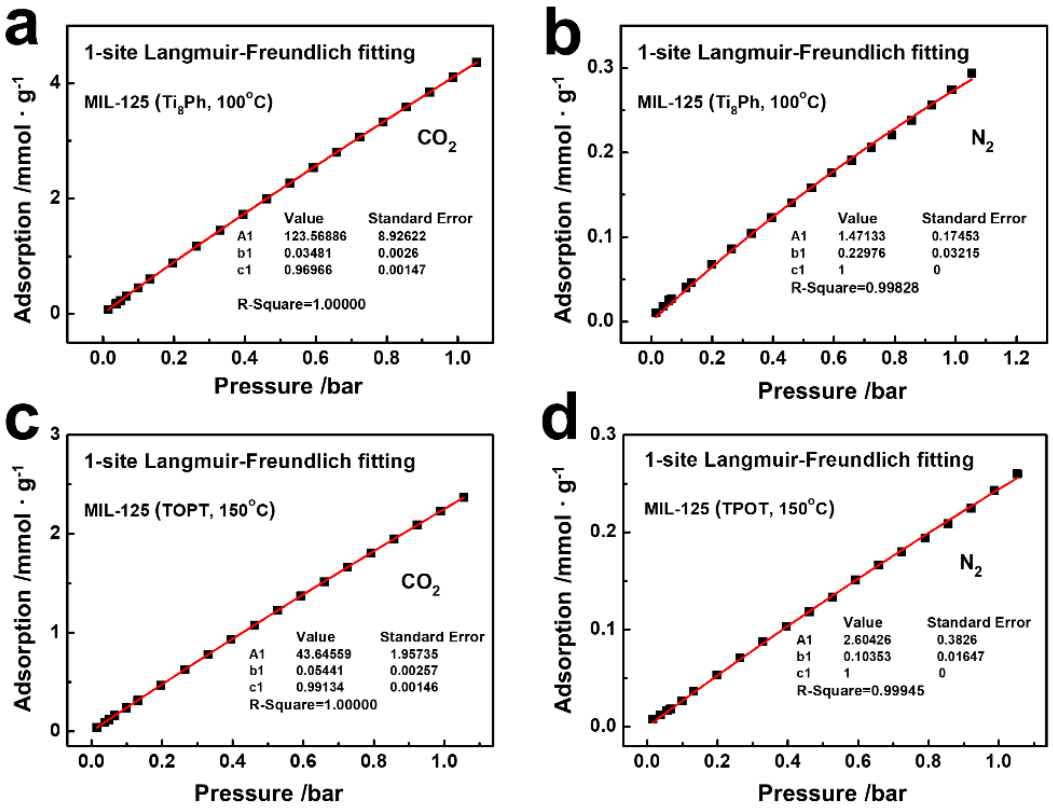

Figure S4. 1-site Langmuir-Freundlich fitting curves for CO_2 and N_2 adsorption isotherms of (a, b) MIL-125 (Ti_8Ph, 100 °C) and (c, d) MIL-125 (TPOT, 150 °C) measured at 298 K and 1 bar.

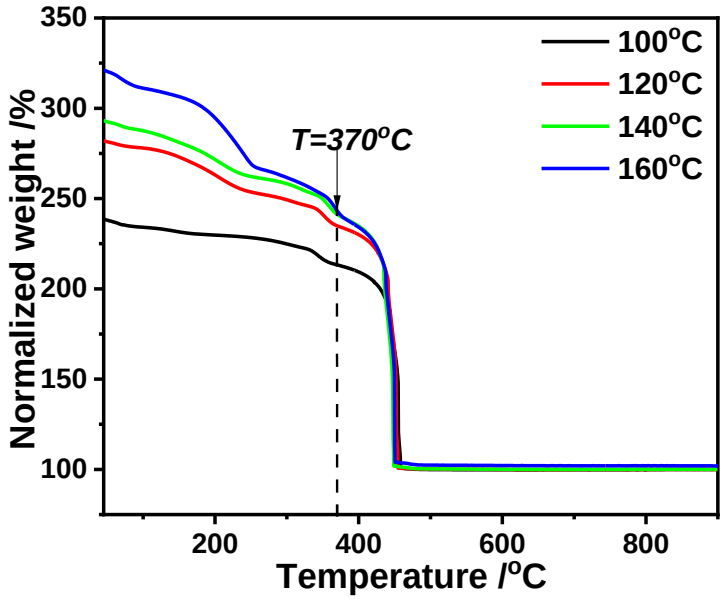

Figure S5. TG curves (normalized to the end weight of TiO_2) of MIL-125 (Ti_8Ph) synthesized at reaction temperatures of 100, 120, 140 and 160 °C under air conditions

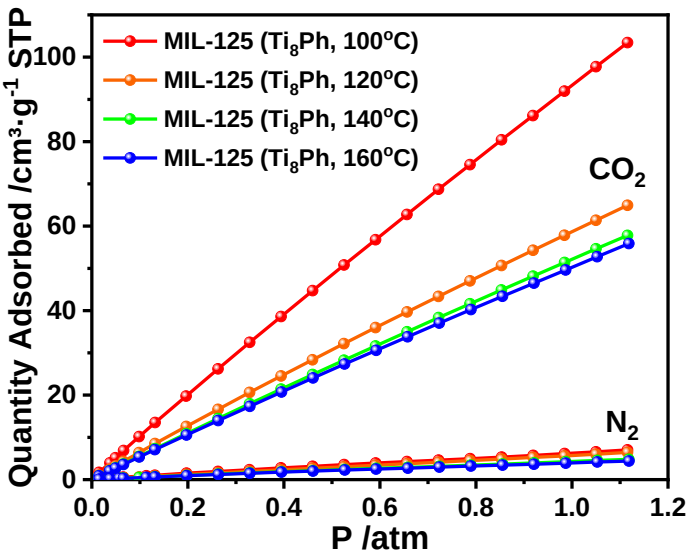

Figure S6. CO_2 and N_2 adsorption isotherms at 298 K of MIL-125 powders prepared by Ti_8Ph cluster source at reaction temperatures of 100, 120, 140 and 160 °C.

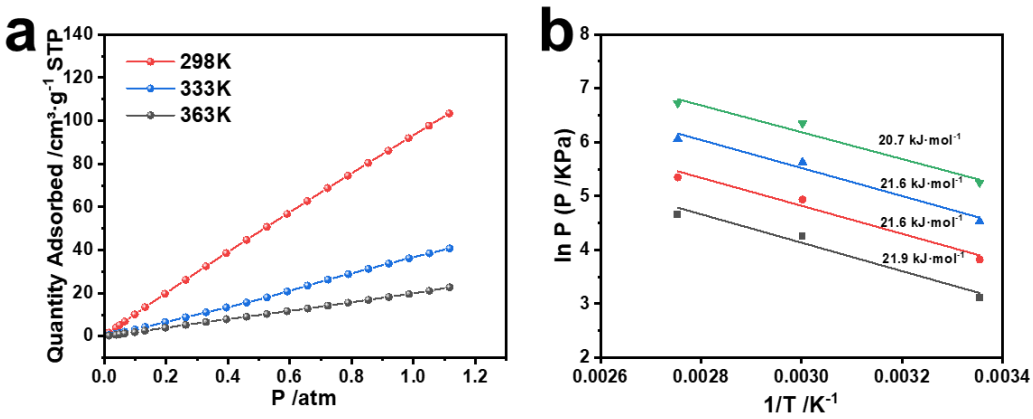

Figure S7. (a) CO_2 adsorption isotherms (from 298 to 363 K) of MIL-125 (Ti_8Ph, 100 °C). (b) CO_2 adsorption isosteres in a temperature range from 298 to 363 K.

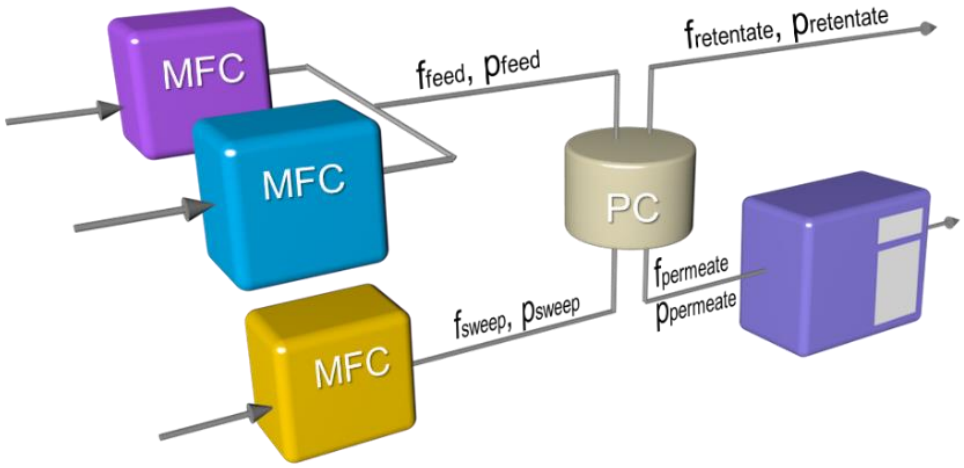

Figure S8. Measurement equipment for single and mixed gas permeation. (MFC: mass flow controller; PC: permeation cell with mounted membrane; GC: gas chromatograph; f: volumetric flow rate; p: pressure). For MIL-125-TG, the stage cut (CO_2) for the CO_2/N_2 mixture at 30 °C was 1.11%.

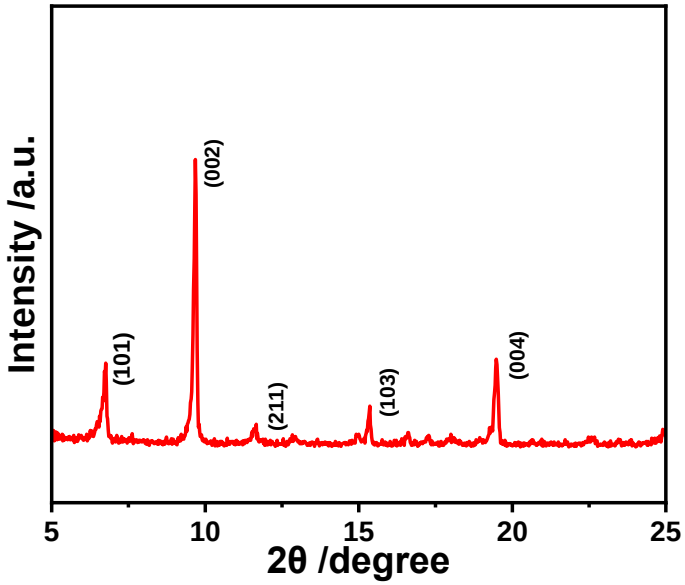

Figure S9. XRD pattern of MIL-125-TG.

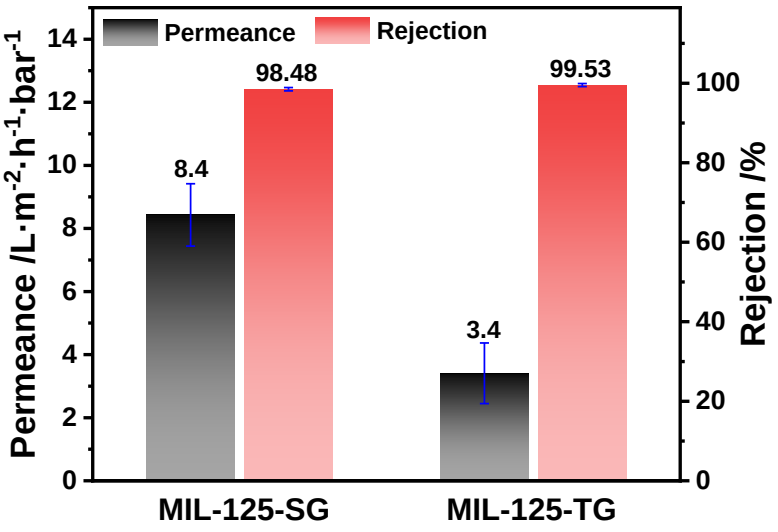

Figure S10. CR dye rejection performance of MIL-125-SG and MIL-125-TG. The CR dye aqueous solution (100 mg·L^{-1}) were applied in the feed side under a pressure of 3 bar at room temperature. Values represent means ± standard deviation for three replicates.

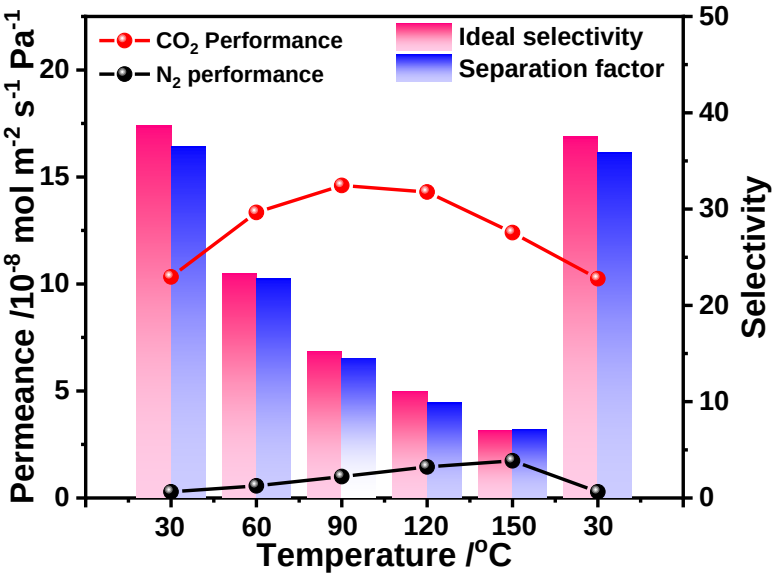

Figure S11. Dependence of gas permeances and CO_2/N_2 selectivity of prepared MIL-125-TG on the operating temperature

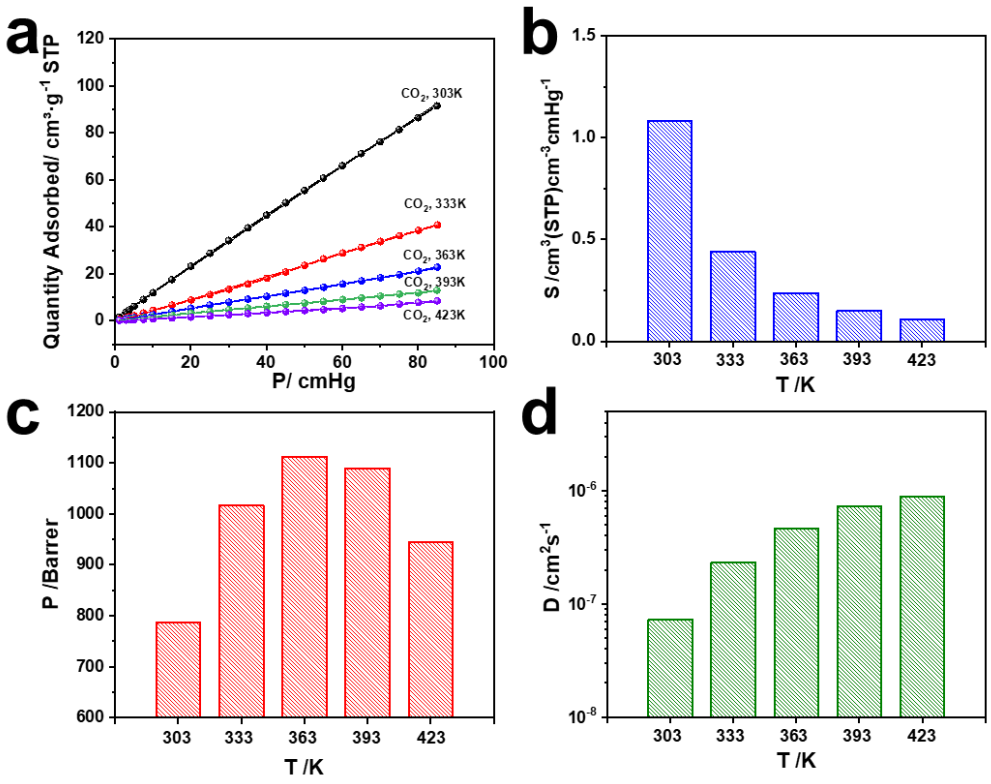

Figure S12. (a) CO_2 adsorption isotherms in a temperature range of 298 to 423K of MIL-125 (Ti_8Ph, 100 ^oC). (b) CO_2 adsorption coefficient, (c) CO_2 permeability, and (d) CO_2 diffusion coefficient of MIL-125-TG in temperature ranges of 303 to 333 K, 333 to 363 K, 363 to 393 K and 393 to 423 K.

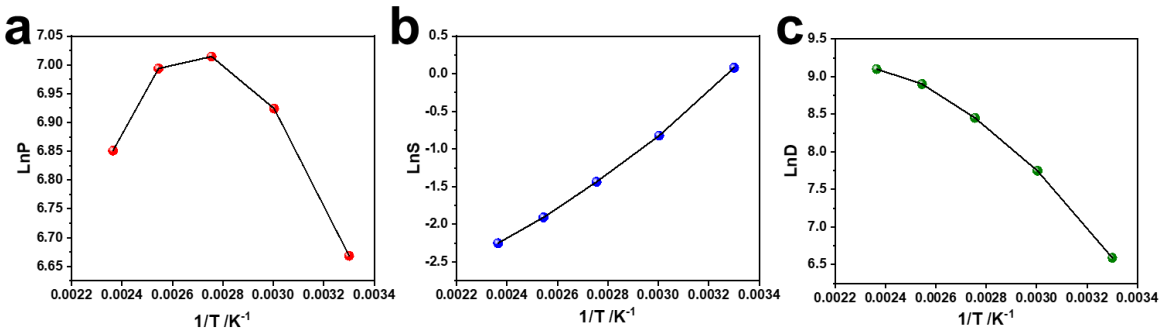

Figure S13. Arrhenius plots for (a) CO_2 permeability, (b) CO_2 adsorption coefficient and (c) CO_2 diffusion coefficient of MIL-125 (Ti_8Ph, 100 ^oC) in temperature ranges of 303 to 333 K, 333 to 363 K, 363 to 393 K and 393 to 423 K.

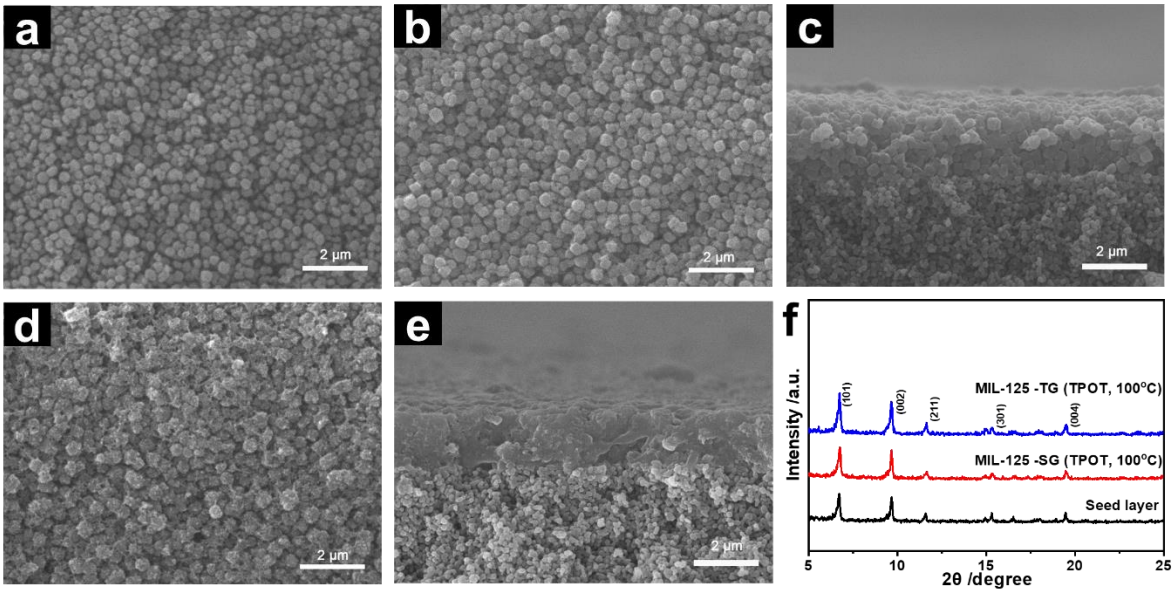

Figure S14. SEM images of (a) the seed layer derived from MIL-125 (TPOT, 150 °C) and corresponding MIL-125 membranes prepared by (b, c) secondary growth and (d, e) tertiary growth using TPOT as Ti source by single-mode microwave heating at 100 °C for 70 min, respectively. (f) The corresponding XRD patterns of above samples.

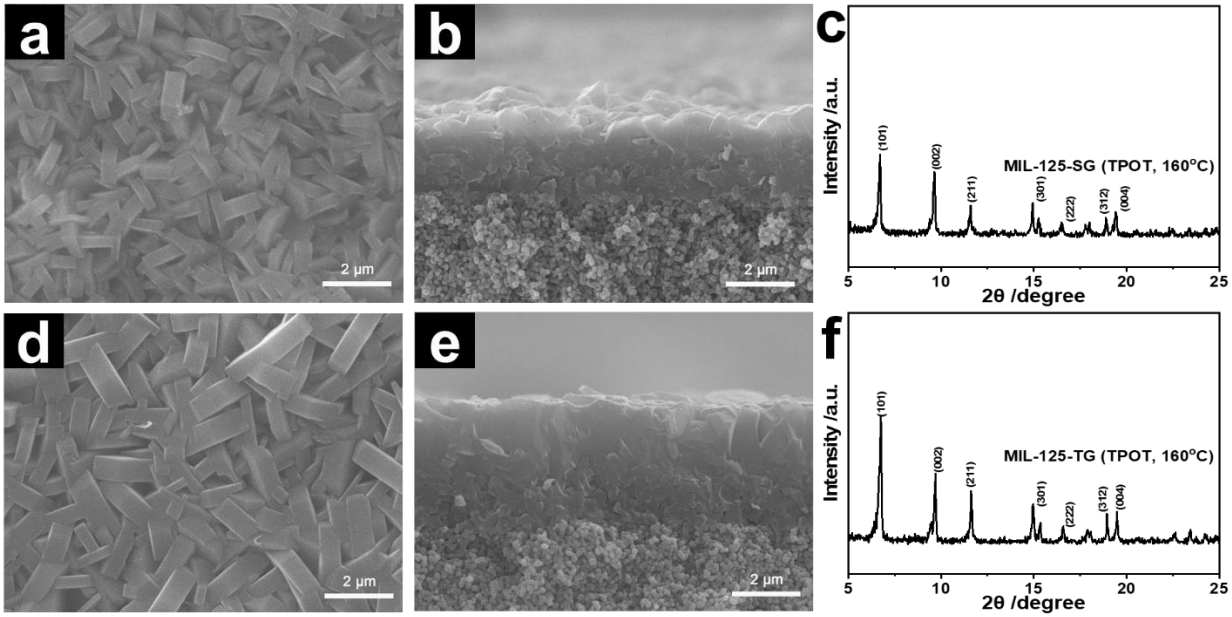

Figure S15. Top and cross-section SEM images as well as corresponding XRD patterns of MIL-125 membranes prepared by (a-c) secondary growth and (d-f) tertiary growth using TPOT as titanium source using single-mode microwave heating at 160 ^{o}C for 10 min.

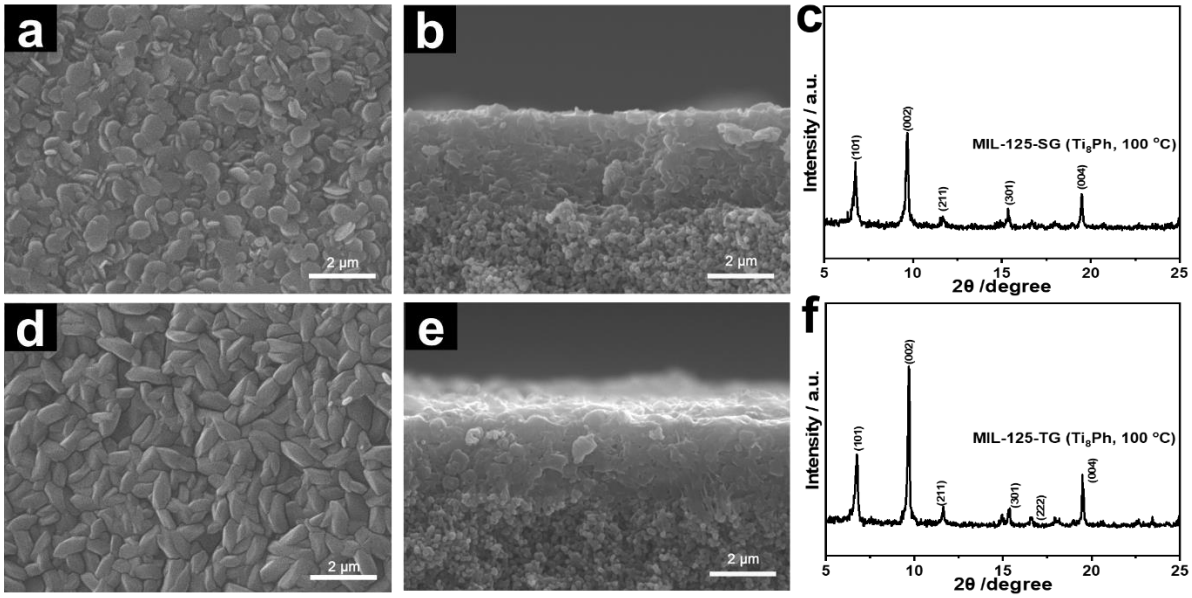

Figure S16. Top and cross-section SEM images as well as corresponding XRD patterns of MIL-125 membranes prepared by (a-c) secondary growth and (d-f) tertiary growth using Ti_8Ph as titanium source using solvothermal heating at 100 °C for 24 h.

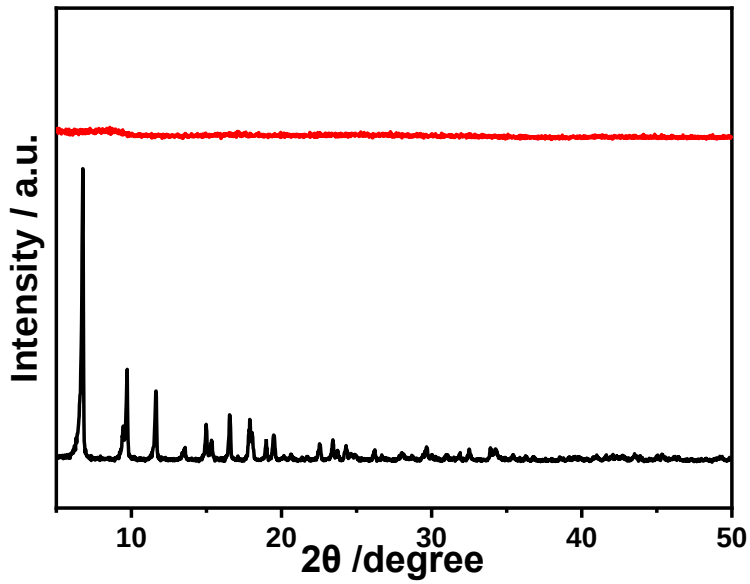

Figure S17. XRD patterns of MIL-125 powders collected at the bottom of the vessel after tertiary growth by solvothermal heating at 100 ºC for 24 h (black line) and single-mode microwave heating at 100 ºC for 70 min (red line).

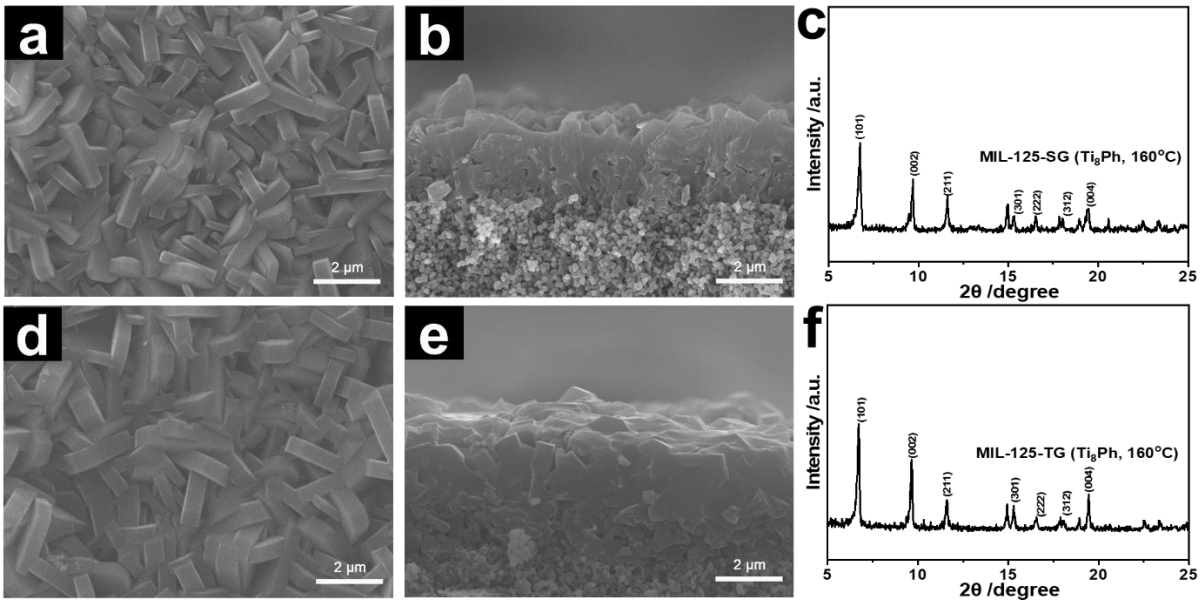

Figure S18. Top and cross-section SEM images as well as corresponding XRD patterns of MIL-125 membranes prepared by (a-c) secondary growth and (d-f) tertiary growth using Ti_8Ph cluster as titanium source with single-mode microwave heating at 160 °C for 10 min.

3.2 Supplementary Tables (Table S1 to S9)

Table S1. Permeances and separation factor of equimolar gas pairs through MIL-125-SG (Ti source: Ti_8Ph cluster) prepared by single-mode microwave heating at 100 °C for 70 min under ambient conditions.

Single gas	H_2	N_2	CO_2	CH_4
Permeance (10^{-8} mol·m^{-2}·s^{-1}·Pa^{-1})	78	5.23	58.7	7.41
Ideal selectivity	H_2/N_2: 15.4			
	CO_2/N_2: 11.5			
	H_2/CH_4: 10.9			

Table S2 Permeance and separation factor of equimolar gas pairs through MIL-125-TG (Ti source: Ti_8Ph cluster) prepared by single-mode microwave heating at 100 ^oC for 70 min under ambient conditions.

Single gas	H_2	N_2	CO_2	CH_4
Permeance (10^{-8} mol·m^{-2}·s^{-1}·Pa^{-1})	20.5	0.32	12.4	0.515
Ideal selectivity	H_2/N_2: 64.9			
	CO_2/N_2: 38.7			
	H_2/CH_4: 40.7			

Table S3. Comparison of the CO_2/N_2 separation performance of prepared MIL-125-TG with other pristine polycrystalline MOF membranes measured under similar conditions.

Membrane	Thickness (μm)	CO_2 permeance (10^{-9}·mol·m^{-2}·s^{-1}·Pa^{-1})	CO_2 permeability (Barrer)	selectivity
CAU-1[3]	2	730	4380	20.3
ZIF-7[4]	2.4	0.81	5.832	13.6
ZIF-8_RHT[5]	0.55	40	66	37.3
ZIF-69[6]	40	103.4	12412.8	6.3
UiO-66[7]	3.5	37.6	393.1	31.3
UiO-66[8]	0.8	580	1385.8	26.5
UiO-66[9]	2	950	5674.7	29.7
UiO-66[10]	2.2	407	2674.3	35.6
HKUST-1[11]	10	90	2700	14.23
sod-ZMOF-1[12]	35	0.63	66.15	8.7
$Ni_3(HITP)_2$[13]	0.6	1590	2862	10.2
$Ni_3(HITP)_2$[14]	0.3	3150	2835	13.8
$Cu(dhbc)_2(bpy)$[15]	0.1	381.3	114.4	28.6
MIL-125-TG	2.54	124.1	788.67	38.7

Table S4. Comparison of the H_2/N_2 separation performance of prepared MIL-125-TG with other pristine 3D MOF membranes measured under ambient conditions.

Membrane	Thickness (μm)	H_2 permeance (10^{-9}·mol·m^{-2}·s^{-1}·Pa^{-1})	H_2 permeability (Barrer)	selectivity
HKUST-1[16]	5-10	1270	19050	4.6
HKUST-1[17]	25	1000	75000	7.5
MMOF[18]	20	470	28200	23
ZIF-7[19]	1.5	74	333	6.73
ZIF-7[20]	2	45.5	273	20.7
ZIF-8[21]	42	60.4	7610.4	11.6
ZIF-22[22]	40	202	24240	7.1
ZIF-67[23]	5	227.5	3412.5	21.8
ZIF-78[24]	25	102	7650	6.6
ZIF-90[25]	20	248	14880	12.6
UiO-66[10]	2.2	203.8	1345.08	18.35
UiO-66[7]	3.5	12.5	131.25	18.1
UiO-66-NH_2[26]	7.5	2770	62325	3.02
NH2-MIL-125 (Ti)[27]	0.5	133.5	66.75	10.4
ZIF-8[28]	1.2	1810	6516	8.5
MIL-125-TG	2.54	205	1562.1	64.9

Table S5. Comparison of the H_2/CH_4 separation performance of prepared MIL-125-TG with other pristine 3D MOF membranes measured under ambient conditions.

Membrane	Thickness (μm)	H_2 permeance (10^{-9}·mol·m^{-2}·s^{-1}·Pa^{-1})	H_2 permeability (Barrer)	selectivity
ZIF-8[29]	20	140	8400	12
ZIF-8[30]	5	102	1530	40.1
ZIF-67[31]	3	1480	13320	18
ZIF-67[23]	5	227.5	3412.5	45.4
ZIF-7_{22}-8[32]	0.5	27.5	41.25	71
ZIF-7_{23}-8[33]	1-2	300	900	21.3
UIO-66[34]	2.6	530	4134	12.9
UIO-66[7]	3.5	14.8	155.4	7.2
NH_2-MIL-Al (53)[35]	15	2671	120195	20.7
NH_2-MIL-125(Ti)[27]	0.5	133.5	66.75	11.2
MIL-125-TG	2.54	205	1562.1	40.7

Table S6. The CO_2 permeation activation energy (E_P), heats of adsorption ($-\Delta H$), and diffusion activation energy (E_D) of MIL-125 (Ti_8Ph, 100 °C) in temperature ranges of 303 to 333 K, 333 to 363 K, 363 to 393 K, and 393 to 423 K.

Temperature interval (K)	E_P (kJ·mol^{-1})	$-\Delta H$ (kJ·mol^{-1})	E_D (kJ·mol^{-1})
303~333 K	7.15	25.22	32.37
333~363 K	3.02	20.54	23.56
363~393 K	-0.82	18.63	17.81
393~423 K	-6.57	15.77	9.20

Table S7. Permeances and separation factor of equimolar gas pairs through MIL-125 membrane (Ti source: TPOT) prepared by secondary growth using single-mode microwave heating at 160 °C for 10 min under ambient conditions.

Single gas	H_2	N_2	CO_2	CH_4
Permeance (10^{-8} mol·m^{-2}·s^{-1}·Pa^{-1})	86	24.9	115.6	70.4
Ideal selectivity	H_2/N_2: 3.5			
	CO_2/N_2: 4.8			
	H_2/CH_4: 1.2			

Table S8. Permeances and separation factor of equimolar gas pairs through MIL-125 membrane (Ti source: TPOT) prepared by tertiary growth using single-mode microwave heating at 160 °C for 10 min under ambient conditions.

Single gas	H_2	N_2	CO_2	CH_4
Permeance (10^{-8} mol·m^{-2}·s^{-1}·Pa^{-1})	50.9	9.65	67.5	33.2
Ideal selectivity	H_2/N_2: 5.3			
	CO_2/N_2: 7.0			
	H_2/CH_4: 1.5			

Table S9. Permeances and separation factor of equimolar gas pairs through MIL-125 membrane (Ti source: Ti_8Ph cluster) prepared by tertiary growth using single-mode microwave heating at 160 °C for 10 min under ambient conditions.

Single gas	H_2	N_2	CO_2	CH_4
Permeance (10^{-8} mol·m^{-2}·s^{-1}·Pa^{-1})	80	8.85	73.4	16.06
Ideal selectivity	H_2/N_2: 9.0			
	CO_2/N_2: 8.3			
	H_2/CH_4: 5.2			

4 References

[1] T. Frot, S. Cochet, G. Laurent, C. Sassoye, M. Popall, C. Sanchez, L. Rozes, *Eur. J. Inorg. Chem.***2010**, *2010*, 5650-5659.
[2] G. C. Shearer, S. Chavan, S. Bordiga, S. Svelle, U. Olsbye, K. P. Lillerud, *Chem. Mater.* **2016**, *28*, 3749-3761.
[3] H. Yin, J. Wang, Z. Xie, J. Yang, J. Bai, J. Lu, Y. Zhang, D. Yin, J. Y. Lin, *Chem. Commun. (Camb)* **2014**, *50*, 3699-3701.
[4] F. Cacho-Bailo, S. Catalán-Aguirre, M. Etxeberría-Benavides, O. Karvan, V. Sebastian, C. Téllez, J. Coronas, *J. Membr. Sci.* **2015**, *476*, 277-285.
[5] D. J. Babu, G. He, J. Hao, M. T. Vahdat, P. A. Schouwink, M. Mensi, K. V. Agrawal, *Adv. Mater.* **2019**, *31*, 1900855.
[6] Y. Liu, G. Zeng, Y. Pan, Z. Lai, *J. Membr. Sci.* **2011**, *379*, 46-51.
[7] R. Rong, Y. Sun, T. Ji, Y. Liu, *J. Membr. Sci.* **2020**, *610*, 118275.
[8] W. Wu, Z. Li, Y. Chen, W. Li, *Environ. Sci. Technol.* **2019**, *53*, 3764-3772.
[9] X. Liu, N. K. Demir, Z. Wu, K. Li, *J. Am. Chem. Soc.* **2015**, *137*, 6999-7002.
[10] J. Yan, Y. Sun, T. Ji, L. Liu, M. Zhang, Y. Liu, *J. Membr. Sci.* **2021**, *635*, 119515.
[11] M. N. Shah, M. A. Gonzalez, M. C. McCarthy, H.-K. Jeong, *Langmuir* **2013**, *29*, 7896-7902.
[12] B. A. Al-Maythalony, O. Shekhah, R. Swaidan, Y. Belmabkhout, I. Pinnau, M. Eddaoudi, *J. Am. Chem. Soc.* **2015**, *137*, 1754-1757.
[13] S. Jiang, X. Shi, Y. Zu, F. Sun, G. Zhu, *Materials Chem. Front.* **2021**, *5*, 5150-5157.
[14] S. Jiang, X. Shi, F. Sun, G. Zhu, *Chem. Asian J.* **2020**, *15*, 2371-2378.
[15] Y. Ying, Z. Zhang, S. B. Peh, A. Karmakar, Y. Cheng, J. Zhang, L. Xi, C. Boothroyd, Y. M. Lam, C. Zhong, D. Zhao, *Angew. Chem. Int. Ed.* **2021**, *60*, 11318-11325.
[16] H. Guo, G. Zhu, I. J. Hewitt, S. Qiu, *J. Am. Chem. Soc.* **2009**, *131*, 1646-1647.
[17] V. V. Guerrero, Y. Yoo, M. C. McCarthy, H.-K. Jeong, *J. Mater. Chem.* **2010**, *20*, 3938-3943.
[18] R. Ranjan, M. Tsapatsis, *Chem. Mater.* **2009**, *21*, 4920-4924.
[19] Y.-S. Li, F.-Y. Liang, H. Bux, A. Feldhoff, W.-S. Yang, J. Caro, *Angew. Chem. Int. Ed.* **2010**, *49*, 548-551.
[20] Y. Li, F. Liang, H. Bux, W. Yang, J. Caro, *J. Membr. Sci.* **2010**, *354*, 48-54.
[21] H. Bux, F. Liang, Y. Li, J. Cravillon, M. Wiebcke, J. Caro, *J. Am. Chem. Soc.* **2009**, *131*, 16000-16001.
[22] A. Huang, H. Bux, F. Steinbach, J. Caro, *Angew. Chem. Int. Ed. Engl.* **2010**, *49*, 4958-4961.
[23] P. Nian, Y. Li, X. Zhang, Y. Cao, H. Liu, X. Zhang, *ACS Appl. Mater. Interfaces* **2018**, *10*, 4151-4160.
[24] X. Dong, K. Huang, S. Liu, R. Ren, W. Jin, Y. S. Lin, *J. Mater. Chem.* **2012**, *22*, 19222-19227.
[25] A. Huang, W. Dou, J. Caro, *J. Am. Chem. Soc.* **2010**, *132*, 15562-15564.
[26] A. Micero, T. Hashem, H. Gliemann, A. Léon, *Membranes* **2021**, *11*, 735.
[27] Y. Sun, Y. Liu, J. Caro, X. Guo, C. Song, Y. Liu, *Angew. Chem. Int. Ed. Engl.* **2018**, *57*, 16088-16093.
[28] M. He, Y. Zhang, Y. Wang, X. Wang, Y. Li, N. Hu, T. Wu, F. Zhang, Z. Dai, X. Chen, H. Kita, *Sep. Purif. Technol.* **2021**, *275*, 119109.
[29] Y. Liu, N. Wang, J. H. Pan, F. Steinbach, J. Caro, *J. Am. Chem. Soc.* **2014**, *136*, 14353-14356.
[30] Y. Li, C. Ma, P. Nian, H. Liu, X. Zhang, *J. Membr. Sci.* **2019**, *581*, 344-354.
[31] Z. Zhou, C. Wu, B. Zhang, *Ind. Eng. Chem. Res.* **2020**, *59*, 3182-3188.
[32] Q. Hou, Y. Wu, S. Zhou, Y. Wei, J. Caro, H. Wang, *Angew. Chem. Int. Ed.* **2019**, *58*, 327-331.
[33] F. Hillman, J. Brito, H.-K. Jeong, *ACS Appl. Mater. Interfaces* **2018**, *10*, 5586-5593.
[34] S. Friebe, B. Geppert, F. Steinbach, J. Caro, *ACS Appl. Mater. Interfaces* **2017**, *9*, 12878-12885.
[35] F. Zhang, X. Zou, X. Gao, S. Fan, F. Sun, H. Ren, G. Zhu, *Adv. Funct. Mater.* **2012**, *22*, 3583-3590.

5 Author Contributions

Y.Liu* conceived the idea and designed the experiments. C.Wang performed major experiments and analyzed the experimental data. Y. Sun gave advice and helped analyze experimental data. L. Li helped with the calculation of gas separation IAST. R. Krishna helped with the calculation and simulation of gas separation IAST. T.Ji helped with the EDXS mapping images. S. Chen helped with the SEM image of the substrate. J. Yan gave relevant literatures. Y.Liu* and C.Wang co-wrote the manuscript with contributions from all authors.